# 9

#### Review

Kwok Kwan Tang, Chun Li, Changhai Zhu, Peipei Li, Liyun Zhao\* and Qing Zhang\*

# Emergent 2D van der Waals materials photonic sources

https://doi.org/10.1515/nanoph-2024-0702 Received November 30, 2024; accepted February 14, 2025; published online March 11, 2025

**Abstract**: Over the past two decades, two-dimensional (2D) van der Waals (vdW) semiconductors have garnered significant attention in the field of light sources due to their unique optoelectronic properties, such as high excitonic binding energy, tunable bandgaps, and strong optical anisotropy. These properties make 2D vdW semiconductors highly promising for next-generation light sources, offering advantages like enhanced efficiency, wavelength tunability, and polarization control. In this review, we summarize the development of various 2D vdW material-based light sources and their modulation mechanisms. We first provide an overview of excitonic properties and light-emission principles that aim to develop light sources with low-power, high-efficiency. Next, we discuss advances in 2D semiconductor lasers, including intralayer and interlayer exciton lasers, cavity-free systems, and exciton-polariton sources. We then look into single-photon emission and their integration into on-chip systems, followed by studies on nonlinear optical properties like high-order harmonic generation and P-band emission. Additionally, we cover advancements in electrically pumped light sources. The review concludes with an outlook on future developments of 2D vdW semiconductor light sources.

\*Corresponding authors: Liyun Zhao, International School for Optoelectronic Engineering, Qilu University of Technology (Shandong Academy of Sciences), Jinan 250353, China, E-mail: zhaoly@qlu.edu.cn;

and **Qing Zhang**, School of Materials Science and Engineering, Peking University, Beijing 100871, China,

E-mail: q\_zhang@pku.edu.cn. https://orcid.org/0000-0002-6869-0381 **Kwok Kwan Tang and Chun Li**, School of Materials Science and Engineering, Peking University, Beijing 100871, China

**Changhai Zhu**, School of Materials Science and Engineering, Peking University, Beijing 100871, China; and School of Physics and Electronic Engineering, Chongqing Normal University, Chongqing 401331, China

**Peipei Li**, School of Materials Science and Engineering, Peking University, Beijing 100871, China; and International School for Optoelectronic Engineering, Qilu University of Technology (Shandong Academy of Sciences), Jinan 250353, China

**Keywords:** 2D van der Waals semiconductors; light sources; exciton; exciton-polariton; nonlinear optics

#### 1 Introduction

Currently, the light source field is advancing toward high-efficiency and low-power consumption, tunable light sources, miniaturization and integration, application of new materials, flexible and wearable devices, nanophotonics and plasmonics, and quantum light sources - all of which are crucial for modern communication, display, and energy applications. Two-dimensional (2D) materials offer unique advantages in developing light sources due to their direct bandgap properties [1], high excitonic binding energy [2], tunable bandgaps [3], strong optical anisotropy [4], high mechanical flexibility and transparency [5], ability to form van der Waals (vdW) heterostructures [6], and compatibility with existing manufacturing processes [7]. These characteristics make 2D vdW materials highly promising for next-generation high-performance, low-power, and multifunctional light sources. This field, pioneered by the discovery of graphene [8], has since expanded rapidly to other promising 2D vdW materials like transition-metal dichalcogenides (TMDs), black phosphorus (BP), and hexagonal boron nitride (hBN), each offering distinct advantages for optoelectronic applications [9]. Monolayer TMDs, for example, including MoS<sub>2</sub> and WS<sub>2</sub>, exhibit direct bandgaps [1], [3], [10] - unlike their bulk counterparts, which are indirect – resulting in enhanced photoluminescence (PL) and thus making them ideal for light emitting diodes (LEDs) [11] and nanolasers [12]. The atomically thin structure and unique optical properties of 2D vdW materials position them as prime candidates for low-power, high-efficiency electronic and optoelectronic devices, particularly where miniaturization is crucial [13]-[16]. Furthermore, a particularly exciting application of 2D semiconductors is in singlephoton sources, which are integral to quantum information science. Single-photon sources technology utilizing 2D vdW materials, such as TMDs and hBN, allows for on-demand single-photon generation with high purity and efficiency

[17]-[20]. For instance, hBN defects are capable of producing stable, room-temperature single-photon emissions (SPEs), making them promising for quantum optoelectronics [17] and quantum sensor [21]. With the growing need for compact, scalable, and high-performance quantum photonic systems, single-photon sources based on 2D vdW materials offers an exceptional pathway for integrating quantum capabilities with traditional photonic devices. Additionally, 2D semiconductors exhibit nonlinear optical phenomena such as high-order harmonic generation (HHG) and P-band emission, which hold significant promise for the development of tunable, integrable light sources, on-chip photonic circuits, ultrafast lasers, and advanced signal processing technologies [22]–[26]. For example, the  $\gamma$ -phase structure of InSe, characterized by its out-of-plane dipole orientation, enhances the efficiency of exciton scattering, enabling Pband emission at low excitation densities [27]. This nonlinear optical behavior in 2D vdW materials opens new avenues for photonic technologies that are both adaptable and compact, addressing critical needs in modern electronics and photonics.

In this review, we systematically summarize various types of light sources based on 2D layered vdW materials and their modulation mechanisms. First, we will provide a brief overview of the exciton properties and lightemission principles of vdW materials. Second, we will discuss the development of 2D semiconductor lasers, including recent advancements in intralayer and interlayer exciton lasers, lasers that operate without external cavities, and exciton-polariton (EP) emission sources. Third, we introduce research on SPE sources based on 2D vdW materials, with an emphasis on their integration into on-chip systems. Fourth, we will describe studies on the nonlinear optical properties of vdW materials, covering HHG and modulation, as well as P-band emission. Fifth, we will discuss the research and advancements in electrically pumped light sources based on vdW materials. Finally, we will offer an outlook on the future development of vdW materials light sources.

# 2 Emission properties of 2D vdW semiconductors

The development of novel light sources based on 2D vdW semiconductors begins with the revelation of their fundamental emission properties, which are strongly linked to their electronic and excitonic states. To achieve high brightness emission, materials with direct bandgap transitions are of primary focus. The most widely studied system is the monolayer of 2H-phase TMDs, which are stable under ambient conditions and exhibit direct bandgap characteristics at the K point in the Brillouin zone, with transition energies in the visible to near-infrared spectral range [10]. As the number of layers increases, interlayer coupling strengthens, shifting the valence band maximum from the K point to the  $\Gamma$  point, thereby changing the material to an indirect bandgap [3]. Because bright emission originates only from direct transitions in TMD monolayers and there is a lack of tunability in thickness, other bulk materials exhibiting direct bandgaps, such as PbI<sub>2</sub>, InSe, NiPS<sub>3</sub>, and CrSBr, have also been explored as emitters [28]-[31]. Nonetheless, these ultrathin materials can typically be regarded as 2D systems, exhibiting characteristics distinctly different from their bulk 3D counterparts. One of the most important features is that as the material thickness decreases, the Coulomb interaction between electrons and holes is enhanced due to the weakened dielectric screening and strong geometric confinement, leading to a series of tightly bound excitonic states (Figure 1a) [2]. In 2H-phase TMD monolayers, the binding energy of 2D excitons can reach several hundred meV, approximately 30 % of the bandgap energy, significantly higher than that of traditional III-V and II-VI semiconductors, and an order of magnitude greater than that of their bulk counterparts (Figure 1b) [32]-[43]. Additionally, some bulk materials with flat electronic bands due to lattice anisotropy (e.g., CrSBr) can also enable strongly localized excitons with a giant bulk exciton binding energy comparable to those of monolayer materials [43].

Another important feature of TMD monolayers is the spin-valley locking phenomenon. The band extrema of TMD monolayers occur at the inequivalent K and K' points in the hexagonal Brillouin zone, where these two valleys exhibit a mirror symmetry due to time-reversal symmetry (Figure 1c) [1]. Due to the strong spin-orbit coupling in transition metal atoms, the spin states in the band structure are split between the K and K' points, with each valley locked to opposite spin directions. As a result, TMD monolayers have two types of energy-degenerate exciton states, which are coupled to right and left circularly polarized light according to the valley optical selection rule [44]-[46]. This additional valley degree of freedom bridges the gap between photonics and spintronics, providing a rich physical basis for achieving novel optical, electronic, and quantum properties [47], [48].

The high spatial overlap of electron-hole wavefunctions in 2D vdW semiconductors generates a strong excitonic transition dipole moment, which means their radiative lifetimes are typically as short as 0.1–10 ps [49]. This short lifetime is not favorable for exciton accumulation and for the long-distance transfer of valley pseudospin

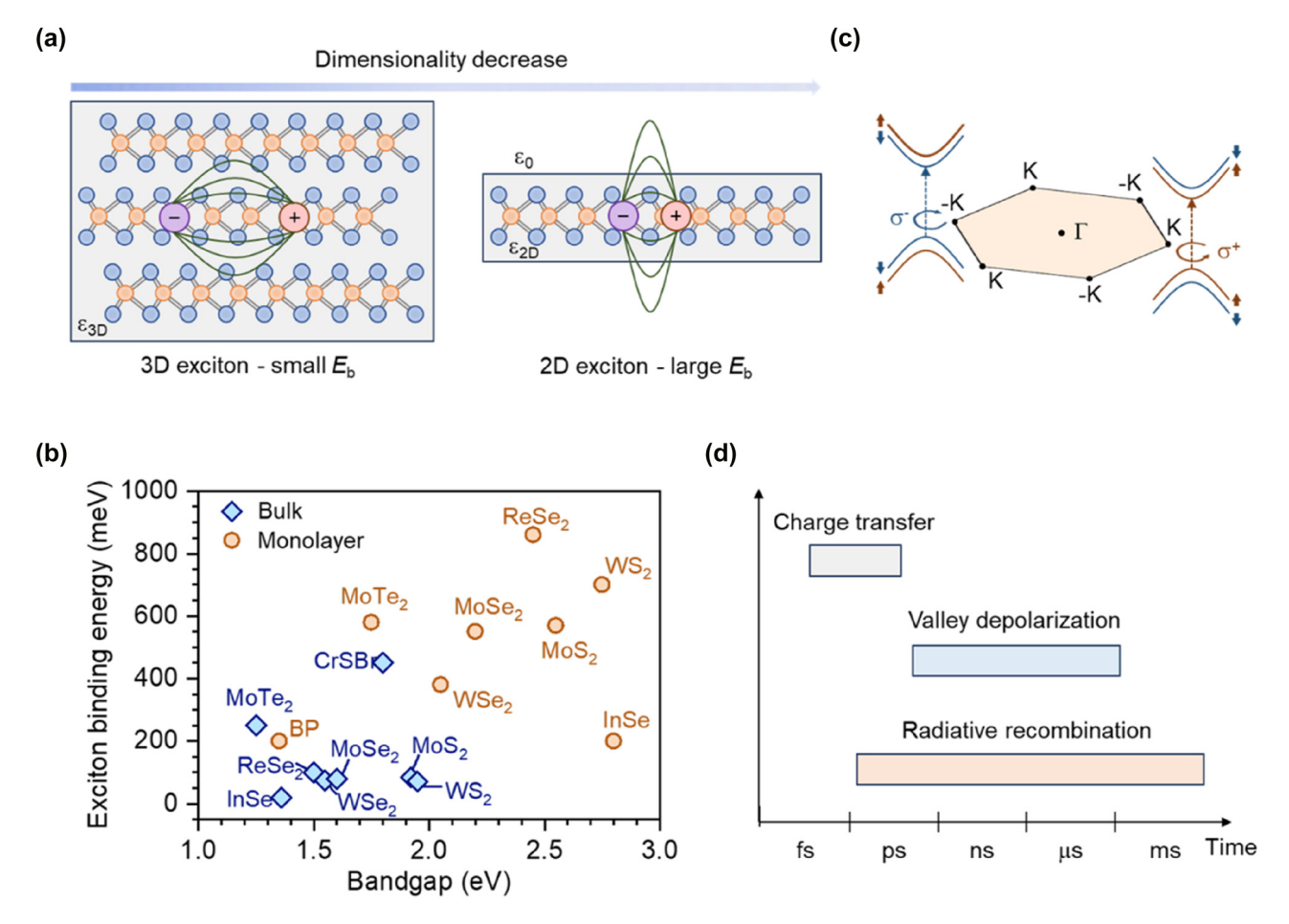


**Figure 1:** Exciton characteristics in 2D van der Waals semiconductors. (a) Schematic of electrons and holes bound into excitons in 3D systems and 2D systems. (b) Exciton binding energy *versus* bandgap for different 2D vdW semiconductors. The data are extracted from refs. [32]–[43], [56]. (c) Schematic of bright excitons at the *K* and *K'* corners of the Brillouin zone of a TMD monolayer, displaying spin-valley locking. (d) Time scale for charge transfer, valley polarization, and radiative recombination in 2D vdW semiconductors.

information. Constructing 2D vdW heterostructures can overcome these limitations. Due to weak interlayer coupling and the absence of surface dangling bonds, different 2D materials can be stacked in any order without disrupting their crystal structures and can tolerate large lattice mismatches, reducing interface defects and ensuring high-quality heterostructures [6]. Atomic-level sharp type-II heterostructures support ultrafast interlayer charge transfer (sub-ps) and allow for spatial separation of electrons and holes across the two layers, thereby suppressing exciton–exciton interactions in both recombination and depolarization processes [50]. As a result, exciton recombination lifetimes can be extended to the ns to ms scale, and valley polarization lifetimes can be extended to the ns to  $\mu s$  scale (Figure 1d) [51]–[55].

For 2D vdW materials and their heterostructures, since bright exciton states dominate the emission process, we further introduce various types of intrinsic many-body complexes of bright excitons that emerge in these systems (Figure 2a). In fact, dark exciton states are also commonly present, and these states cannot be directly excited by light due to the requirement of spin flipping and/or phonon-assisted momentum transfer [57]–[60]. The relative position of the dark exciton states to the optically accessible bright exciton states plays a crucial role in determining the light emission efficiency of these materials and thus technological potential. For a more detailed discussion on dark exciton states, we refer to other reviews [61], [62].

#### 2.1 Neutral exciton

The basic neutral exciton consists of a negatively charged electron and a positively charged hole bound together by Coulomb forces. The electron and hole can originate from a single material, forming intralayer excitons, or can each be provided by separate layers, forming interlayer excitons [41], [51], [63]. Intralayer excitons have a higher binding

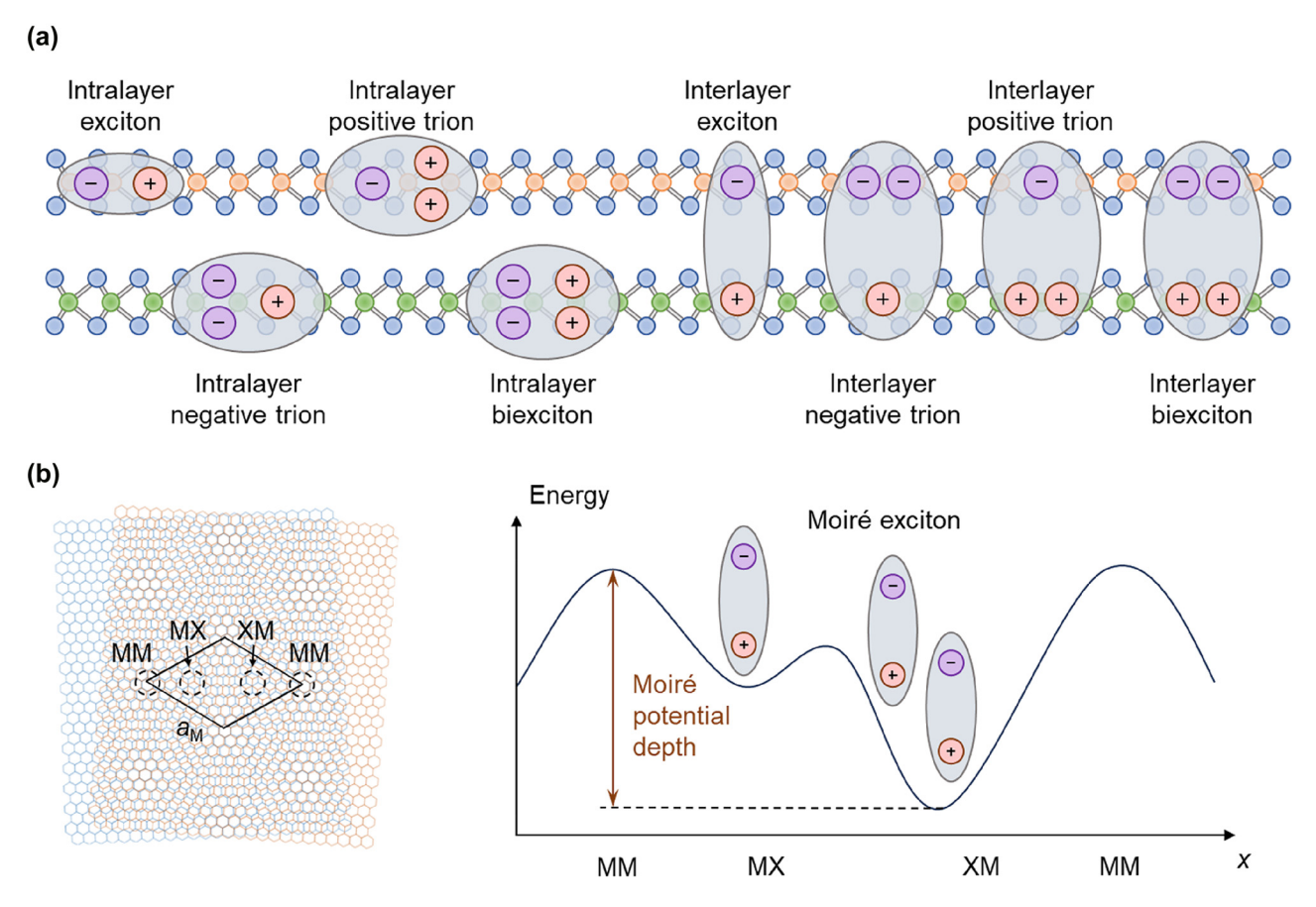


Figure 2: Different types of intralayer and interlayer exciton complexes. (a) Schematic of different types of intralayer and interlayer exciton complexes. (b) Schematic of a moiré superlattice formed by two hexagonal lattice with a small twist angle (left penal) and energy landscape of moiré exciton in the moiré potential (right panel).

energy (>500 meV) and shorter lifetimes (in the picosecond range) because the electron and hole are located within the same layer and are relatively close. In contrast, due to the spatial separation of the electron and hole, interlayer excitons have a slightly smaller binding energy ( $\sim$ 100–300 meV) and longer lifetime extending to the nanosecond scale. Moreover, for vertically stacked heterostructures, interlayer excitons exhibit an out-of-plane transition dipole moment, which is beneficial for creating and manipulating dipole interactions, aiding research on strongly correlated systems, developing tunable optical devices, and realizing exotic physical phenomena such as exciton flux and superfluidity [64]-[66]. A significant spatial overlap between the wavefunctions of intralayer and interlayer excitons will further lead to the mixing of exciton states to form hybrid excitons with optical, electrical, and dynamic properties intermediate between the two. The hybrid nature allows for the customization of the exciton oscillator strength, lifetime, and external field modulation. To facilitate the formation of hybrid excitons, the energy levels in each layer should be close and have the same spin, which has been widely

observed in both homobilayer and heterobilayer systems [67]-[70].

#### 2.2 Trion

When a neutral exciton captures an additional negatively charged electron or positively charged hole, a new charged composite is formed, i.e., a negative or positive trion. The introduction of the additional carrier weakens the manybody interactions and causes the expansion of exciton wavefunction; therefore, the binding energy of trion is usually an order of magnitude lower than that of neutral exciton. The formation of intralayer and interlayer trions depends on specific environmental conditions, such as the doping level, light intensity, temperature, and applied electrical fields, which affect the free carrier density and the exciton capture ability of free carriers. Specifically, interlayer trions include two types: Type I (two identical charges in the same layer) is energetically more favorable and has been reported in most experiments [71]–[73], while Type II (two identical charges in different layers) has also been experimentally verified and exhibits additional polarized emission behavior due to anisotropic charge interactions [74].

#### 2.3 Biexciton

Under extremely high exciton density, efficient inelastic scattering between excitons leads to the formation of a neutral complex consisting of two excitons, known as the biexciton. Intralayer biexcitons have no significant electric dipole moment, while interlayer biexcitons with charge separation occurring across the two layers possess a strong vertical electric dipole moment. Depending on the ratio of exciton spacing to the Bohr radius, biexcitons can be classified into bound and unbound types, where Coulomb attraction dominates in the former (with negative binding energy) and repulsive interactions between individual dipole excitons drive the latter (with positive binding energy [75]–[79]). Bound biexcitons are common in intralayer configurations, while unbound biexcitons are more common in interlayer configurations.

#### 2.4 Moiré exciton

In vdW bilayers, when the monolayers are stacked at a small angle or with lattice mismatch, a long-period spatially periodic structure known as a moiré superlattice is formed (Figure 2b [80], [81]). The moiré superlattice introduces

a periodic in-plane potential landscape at the nanoscale, which can be used to modulate the electronic band structure of the material periodically. Additionally, the periodic modulation can also arise from strain, substrate, or optical field. All excitons mentioned above can be modulated under the periodic potential of the moiré superlattice and can move in the optical lattice, forming moiré excitons when the exciton Bohr radius is smaller than the moiré period [69], [77], [82]–[86]. Moiré excitons exhibit unique optical and electronic properties, such as wavefunction localization at high-symmetry positions within the moiré superlattice, showing quasi-zero-dimensional natures with enhanced stability, flat band dispersion, and significant many-body correlations [87], [88].

In the following sections of this review, we will discuss various emerging 2D vdW semiconductor light sources. Before delving into specific progresses, we will briefly introduce the underlying physical mechanisms associated with these light sources. The fundamental light emission in 2D vdW semiconductors is spontaneous emission (SE), where excited-state carriers, such as electrons and holes, can spontaneously recombine and release photons to return to the ground state (Figure 3a). Besides, the SPE is a special SE process, where only one photon is emitted within a specific time frame, evidenced by the intensity-correlation function at zero time delay  $g^{(2)}(0) < 0.5$  (Figure 3b [20]). The SPE typically arises from localized exciton states induced by

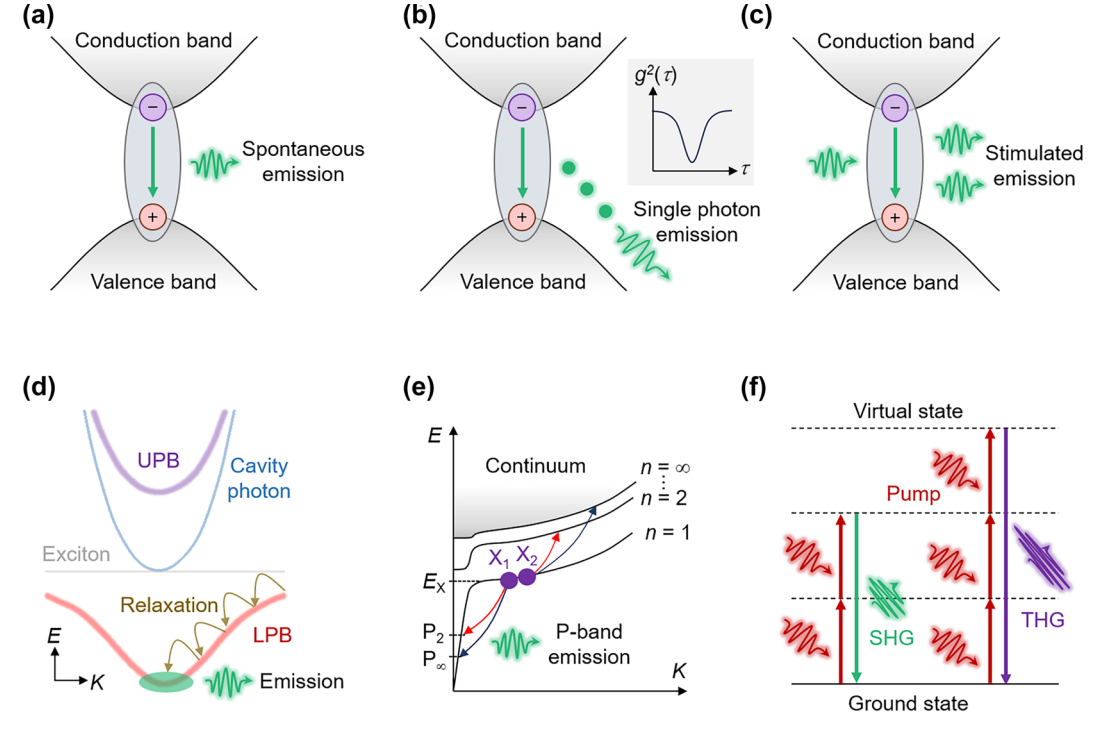


**Figure 3:** Schematic of spontaneous emission (a), SPE (b), stimulated emission (c), EP condensation (d), P-band emission (e), and second/third harmonic generation (f).

strain, electric fields, defects, or moiré periodic potentials. Single-photon sources are one of the core building blocks for photonic integrated circuits used in quantum applications, such as quantum communication and quantum computing. Excited-state carriers can be obtained through optical, electrical, or chemical excitations, and from a practical perspective, this review will focus on LEDs and electrically pumped single-photon sources that utilize electrically driven SE.

Another important light-emitting unit is the laser, which relies on stimulated emission. When an excited-state carrier is stimulated by a photon with energy matching its transition energy, the carrier will transition to the ground state and release a new photon identical to the incident photon, accompanied by light amplification (Figure 3c). Realizing a laser requires a resonant cavity to provide optical feedback, in which excitons couple with cavity photons, typically under the weak coupling regime. When the coupling rate between the excitons and cavity photons exceeds their dissipation rates, a new hybrid quasiparticle, called EP, is created in the strong coupling regime, leading to the splitting of the energy bands into upper and lower polariton branches with anticrossing behavior in energy-momentum dispersion (Figure 3d [89]). The bosonic nature of EPs allows for Bose-Einstein condensation (BEC) at high temperatures, owing to their lighter mass inherited from the photon component, with a large number of EPs occupying the ground state, resulting in photon amplification. The characteristics of EP condensation is very similar to those of conventional lasers, but without the need for population inversion, making them suitable for developing low-threshold laser-like light sources.

To bridge the gap between high-intensity/highcoherence lasers and low-intensity/low-coherence LEDs, high-intensity but low-coherence light sources are also required, which have distinct advantages in applications such as optical coherence tomography, interferometric sensing, and frequency-resolved lidar. One solution is to utilize superlinear P-band emission, which occurs through elastic exciton–exciton scattering in the presence of EPs [90]. Two excitons in the n = 1 exciton state can scatter, with one downward to a lower photon-like polariton state, triggering P-band emission, while the other upward to a higher excited state (n = 2 to  $\infty$ , Figure 3e). The final photon state for P-band emission with negligible interparticle interactions exhibits a narrow linewidth. The scattering process between exciton pairs leads to a quadratic power dependence for P-band emission, eliminating the need for population inversion, which allows for strong light output with low energy consumption.

Finally, we discuss nonlinear light sources based on 2D vdW materials, with a particular focus on the generation of higher-order optical harmonics and frequency conversion through the nonlinear polarization response of 2D vdW materials to an applied optical field (Figure 3f [91]). Compared to traditional bulk nonlinear crystals, 2D vdW materials, benefitting from their ultrathin thickness, relaxed phase matching condition, and larger nonlinear coefficient, open new opportunities for realizing miniaturized on-chip nonlinear photonic and optoelectronic devices.

#### 3 2D semiconductor lasers

2D semiconductor lasers are of particular interest because of their potential applications in nanophotonic, optical communication, and integrated photonic circuits. The development of 2D semiconductor lasers is driven by the unique combination of material properties that these atomiclayer-thin materials offer, including direct bandgaps [1], [3], [10], strong excitonic effects with large exciton binding energy [2], [41], [92], spin-valley locking [44], [45], [93]-[100], and notable charge carrier mobility [13], [101], [102], which are critical for efficient light emission and laser action.

As discussed above, monolayer TMDs exhibit a direct bandgap transition due to the absence of interlayer interactions that typically induce indirect bandgaps in bulk materials. This transition leads to a high radiative recombination quantum efficiency, which is critical for achieving the necessary population inversion in a laser system. TMDs are also distinguished by their strong excitonic effects, arising from their reduced dielectric screening and quantum confinement in two dimensions, which result in an exceptionally high exciton binding energy. This high binding energy allows excitons to remain stable even at room temperature, while also supporting a high Mott transition density ( $\sim 10^{14}$  cm<sup>-2</sup>) [10], preventing thermal dissociation into free carriers, a major advantage over conventional semiconductor lasers. Additionally, the small Bohr radius of excitons in TMDs enhances light-matter coupling, leading to strong oscillator strengths and high optical absorption coefficient, ensuring an efficient stimulated emission process. However, due to their atomically thin nature, TMD monolayers do not provide sufficient optical confinement, necessitating integration with high quality factor (Q-factor) optical cavities to sustain lasing. Various cavity designs, such as photonic crystal cavities (PCCs), which exploit Bragg diffraction to confine light in periodic dielectric structures, whispering-gallery-mode (WGM) resonators, which rely on total internal reflection at curved interfaces to achieve ultrahigh Q-factor, and distributed Bragg reflectors (DBRs), which use multi-layered optical interference to enhance light feedback, all contribute to reducing the threshold carrier density required for lasing.

Unlike intralayer excitons, which form within a single monolayer and exhibit shorter lifetimes and strong recombination, interlayer excitons emerge in type-II band-aligned heterostructures (e.g., MoS<sub>2</sub>/WSe<sub>2</sub>, WSe<sub>2</sub>/MoSe<sub>2</sub>) [103], [104], where electrons and holes reside in separate layers. This spatial separation occurs due to ultrafast charge transfer (~50 fs) following optical excitation, where electrons migrate to the conduction band of one layer while holes remain in the valence band of the other. This configuration results in several key advantages, in detail, (1) longer exciton lifetimes (~µs), which significantly exceed those of intralayer excitons (~ps) [54], allowing for excitonic condensation and lasing buildup; (2) a permanent out-of-plane electric dipole moment, enabling precise control over excitonic energy levels via an external electric field; and (3) reduced recombination rates, improving optical gain efficiency. To achieve interlayer exciton lasing, high-Q optical cavities are employed to provide sufficient optical feedback and enhance the stimulated emission process.

In recent years, significant advancements in 2D semiconductor lasers have been achieved, driven by the unique properties of 2D vdW materials. Key developments include miniaturization and on-chip integration for optical communication and computing systems, room-temperature operation enhancing practical feasibility, and precise tuning of energy bands and optical properties through vdW heterostructures. Enhancements in light-matter interactions have reduced laser thresholds and increased efficiency, while the exploration of new 2D vdW materials has expanded potential applications. Integration with silicon photonics and application-driven research have further propelled the development of high-efficiency, tunable, and easily integrable lasers, profoundly impacting fields such as communication, computing, and sensing. Extensive and indepth studies have been conducted on the lasing properties of various TMD materials integrated within different cavity structures, as well as the lasing characteristics of certain vdW materials without external cavities [12], [103]-[112], as depicted in Figure 4. In this part, we introduce different 2D laser systems with and without external cavities and highlight the special features of EP in these materials.

# 3.1 Intralayer-exciton laser based on monolayer TMD with different cavities

In 2015, Wu et al. demonstrated a continuous-wave (CW) nanolaser by integrating monolayer WSe<sub>2</sub> onto a prefabricated GaP PCC (Figure 5a, top panel) [12]. The hybrid WSe<sub>2</sub>-PCC nanolaser showed lasing at 739.7 nm with a linewidth of 0.3 nm (Figure 5a, bottom panel), and a low lasing threshold power of 27 nW at 130 K, similar to quantum-dot PCC lasers [113]. The high initial *Q*-factor ( = 8,000) enabled a

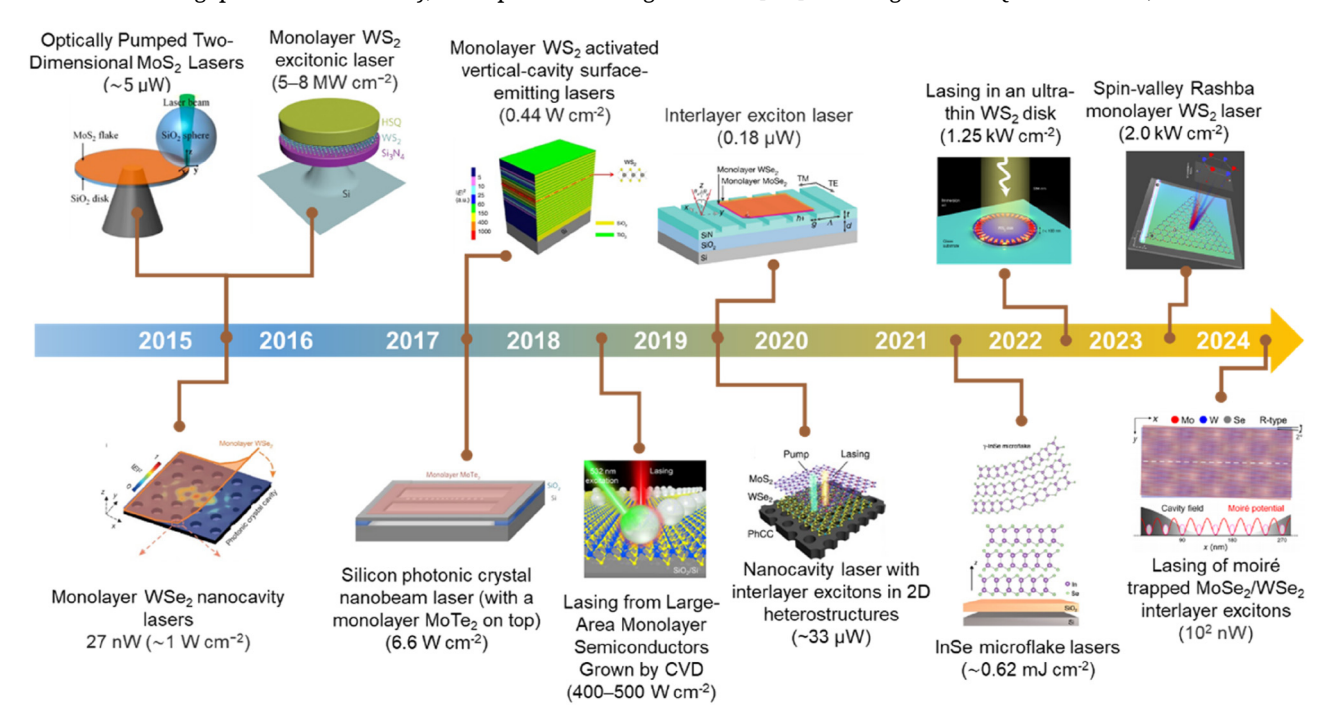


**Figure 4:** A timeline of key advancements in nanophotonics and low-power lasers based on 2D materials from 2015 to 2024. Laser systems with (intralayer exciton complexes [12], [105]–[110], interlayer exciton complexes [103], [104] and moiré exciton complexes [111]) and without external cavity [29], [112].

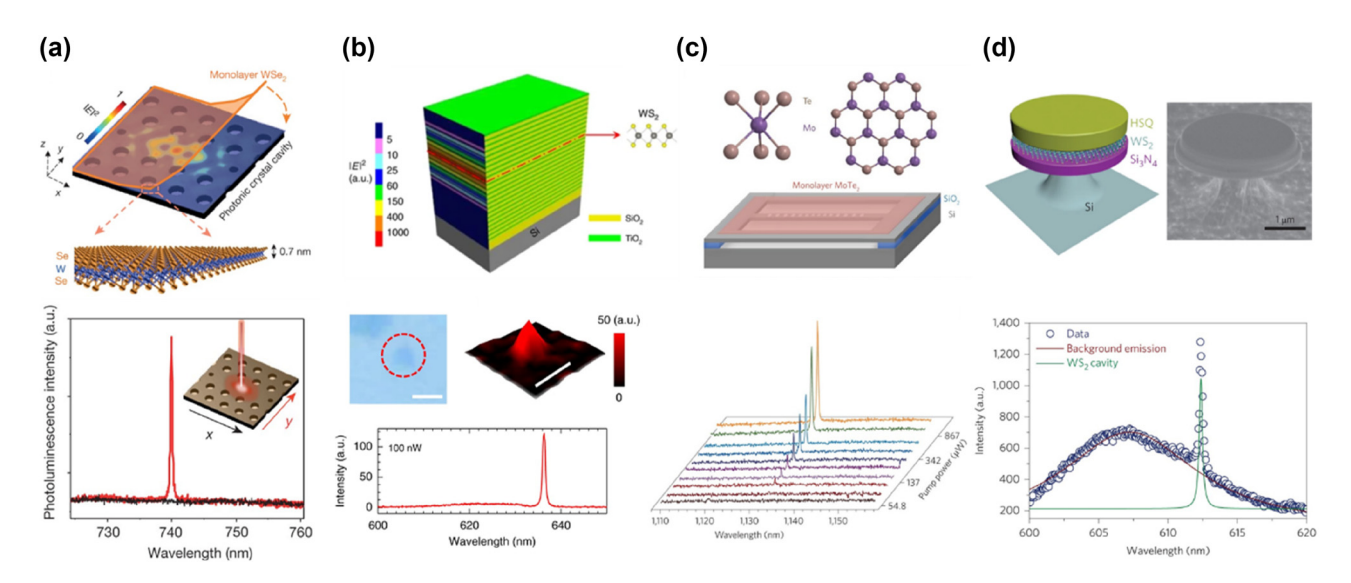


**Figure 5:** Four distinct cavity architectures for TMD-based intralayer exciton lasers. (a) Top panel: the architecture of a hybrid monolayer WSe<sub>2</sub> PCC nanolaser, including a color plot depicting the electric field profile of the fundamental cavity mode (before the WSe<sub>2</sub> transfer). Bottom panel: the polarization-resolved PL spectrum of the nanolaser at 80 K. The black and red lines correspond to detected linear polarizations in the *x* and *y* directions, respectively. Reproduced from ref. [12]. Copyright 2017, Springer Nature. (b) Top panel: the structural schematic of a vertical-cavity surface-emitting laser based on a monolayer of WS<sub>2</sub>. Middle panel: the optical image of monolayer WS<sub>2</sub> (left) and the spatially resolved PL intensity mapping of the microcavity sample (right). The scale bars represent 2 μm. Bottom panel: the PL spectra collected at the center of the sample with an excitation power of 100 nW. Reproduced from ref. [108]. Copyright 2017, Springer Nature. (c) Top panel: the atomic structure of monolayer MoTe<sub>2</sub> and the silicon photonic crystal nanobeam cavity structure with a monolayer of MoTe<sub>2</sub> positioned on top. Bottom panel: the PL spectra at increasing pump power levels, showing the transition from spontaneous to stimulated emission. Reproduced from ref. [107]. Copyright 2017, Springer Nature. (d) Top panel: the schematic (left) and scanning electron microscope image (right) of a monolayer WS<sub>2</sub> microdisk laser, comprising a sandwich structure of Si<sub>3</sub>N<sub>4</sub>/WS<sub>2</sub>/HSQ. Bottom panel: the PL spectrum fitted with bi-Lorentzian curves, separating the monolayer WS<sub>2</sub> PL background (from the microdisk center) from the sharp cavity emission. This distinction highlights the lasing characteristics of the cavity, where the narrow emission peak signifies stimulated emission within the microdisk laser. Reproduced from ref. [106]. Copyright 2015, Springer Nature.

strong Purcell effect [114]–[116], enhancing SE and reducing the lasing threshold. After monolayer transfer, the *Q*-factor reduced to 2,500, but efficient coupling persisted with an SE coupling factor ( $\beta$ ) of 0.19, demonstrating effective emission comparable to quantum-dot PCC lasers [113], [117].

The development of room-temperature, low-threshold vertical-cavity surface-emitting lasers (VCSELs) incorporating 2D semiconductor materials represents a significant step toward practical optoelectronic applications. In 2017, Yu et al. reported a room-temperature CW VCSEL using monolayer WS<sub>2</sub> as the gain medium (Figure 5b, top panel) [108]. The VCSEL employed SiO<sub>2</sub>/TiO<sub>2</sub> DBRs to form a high-reflectivity cavity. The monolayer WS<sub>2</sub>, positioned at the cavity's antinode, maximized light–matter interaction and SE enhancement via the Purcell effect. The laser achieved a low threshold power of 5 nW at 636.3 nm (Figure 5b, bottom panel), with a *Q*-factor of 640.

Silicon's bandgap ( $\sim$ 1.12 eV, 1,100 nm) causes high absorption for emissions above this wavelength [118], [119], making most TMDs unsuitable for integration with silicon cavities. MoTe<sub>2</sub>, with a bandgap greater than 1.7 eV and a PL peak at 1.1 eV, is ideal [39], [120], [121]. In 2017, Li et al. demonstrated CW lasing using monolayer MoTe<sub>2</sub>

integrated with a silicon nanobeam cavity (Figure 5c, top panel) [107]. The cavity achieved a *Q*-factor of 5,603, with lasing at 1,132 nm (linewidth: 0.202 nm, bottom panel of Figure 5c) and a low threshold power density of 6.6 W/cm², which is notably lower than other excitonic lasers in ultraviolet wavelengths operating at room temperature [122]. This design allows efficient lasing at wavelengths where silicon is transparent, making it promising for silicon photonics.

Microdisk resonators are crucial for 2D lasers, supporting WGMs that confine light efficiently [123]. Ye et al. integrated monolayer  $\mathrm{WS}_2$  with a microdisk resonator in 2015, creating a high-quality WGM cavity with a *Q*-factor of 2,604 (Figure 5d, top panel) [106]. The lasing mode at 612.2 nm (Figure 5d, bottom panel), along with additional modes, demonstrated efficient optical confinement with a lasing threshold between 5 and 8 MW/cm². Linewidth narrowing from 0.28 nm to 0.24 nm indicated the lasing onset, and this work demonstrated the potential for valley-selective lasing, offering new functionalities in 2D vdW material-based photonics [94].

Tuning the optical properties of 2D semiconductors is crucial for developing high-performance photonic devices. WGM cavities, with their high *Q*-factor, significantly

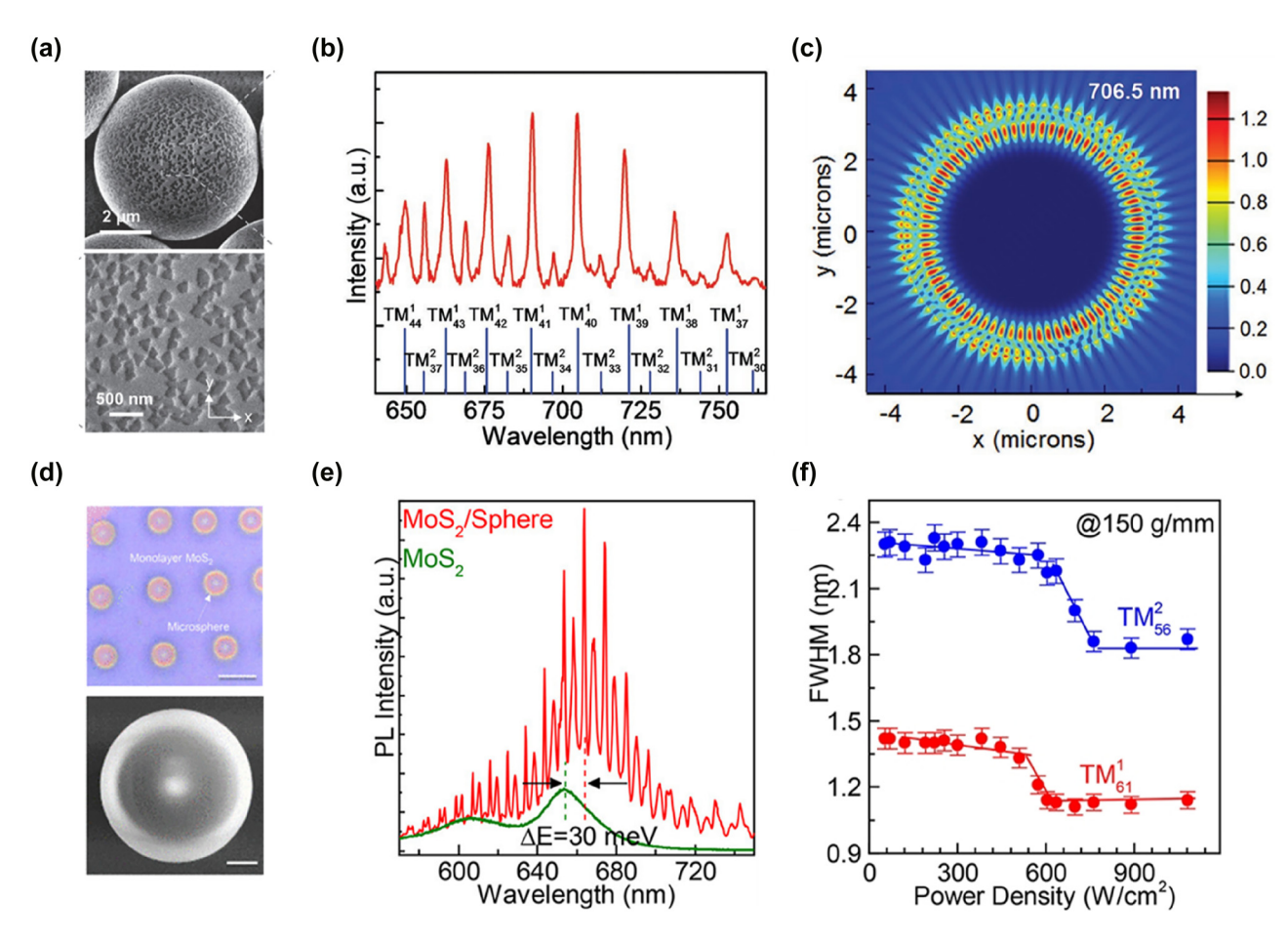


Figure 6: Application of SiO<sub>2</sub> microspheres on 2D TMD materials emission. (a) Top-view scanning electron microscope images of monolayer MoS<sub>2</sub> grown on SiO<sub>2</sub> microspheres at different magnifications. (b) PL spectrum of MoS<sub>2</sub> on a single SiO<sub>2</sub> microsphere, with background emission subtracted to clearly display the WGM resonance peaks. (c) A FDTD simulation, showing the electric field distribution pattern of a transverse magnetic (TM) mode at a resonance wavelength of 706.5 nm in the microcavity. Panel (a-c): reproduced from ref. [128]. Copyright 2017, Wiley-VCH. (d) Upper panel: the optical image of the MoS<sub>2</sub>/microsphere array structure. Lower panel: the scanning electron microscope image of a single SiO<sub>2</sub> microsphere within the array. (e) The PL spectra comparing MoS<sub>2</sub>/microsphere (red line) with monolayer MoS<sub>2</sub> on a SiO<sub>2</sub> – Si substrate (olive line) at room temperature. The higher PL intensity of the MoS<sub>2</sub>/microsphere configuration indicates enhanced emission due to the lensing effect of the microsphere, which focuses excitation light onto the MoS<sub>2</sub> layer more efficiently. (f) The FWHM values for the TM61<sup>1</sup> and TM56<sup>2</sup> modes of the WGM laser as a function of excitation power. The narrowing of the FWHM at higher excitation powers demonstrates the threshold behavior typical of lasing, confirming the WGM laser operation in the MoS<sub>2</sub>/microsphere system. Panel (d-f): reproduced from ref. [109]. Copyright 2018, American Chemical Society.

enhance light-matter interactions, making them ideal for optical amplification and sensing [124]-[127]. Mi et al. used chemical vapor deposition (CVD) to deposit monolayer MoS<sub>2</sub> onto SiO<sub>2</sub> microspheres, forming MoS<sub>2</sub>/SiO<sub>2</sub> microcavities (Figure 6a) [128]. At room temperature, multiple WGM peaks were observed between 650 and 750 nm under CW excitation (Figure 6b), and these peaks were validated through finite-difference time-domain (FDTD) simulations (Figure 6c). These microcavities exhibited refractive index sensing with a sensitivity of 150 nm per refractive index unit, highlighting their potential for optoelectronic sensors. Adjusting the microsphere diameter allowed further tuning of WGM modes to optimize sensing performance.

Traditional 2D vdW material lasers are typically fabricated via mechanical exfoliation, which poses challenges for reproducibility and large-scale production. To overcome this, Zhao et al. grew large-area MoS2 films using CVD and coupled them with SiO2 microspheres to form WGM cavities (Figure 6d) [109]. The microspheres reduced screening effects, enhancing carrier localization and improving effective optical gain [129], [130]. This setup increased exciton SE efficiency (Figure 6e) and enabled strong CW lasing output over a wide temperature range (77-400 K). The devices exhibited low lasing thresholds (32-580 W/cm<sup>2</sup>), which is much lower than that of many traditional laser structures [105]-[107], and the full width at half maximum

of the lasing mode significantly narrowed beyond the threshold (Figure 6f), indicating strong optical gain and stable lasing. These findings demonstrate the potential of microsphere-coupled MoS2 microcavities for developing low-power, wide-temperature-range optical devices.

#### 3.2 Interlayer-exciton laser based on TMD heterobilaver

Previous research has focused on nonlinear lasing behavior and linewidth narrowing in monolayer TMDs [12], [105]-[109]. However, the spatial coherence of the emission has remained unexplored, and the photon flux was observed to be below the stimulated emission threshold, making it complex to rule out localized excitons as the origin of the lasing [131]. Meanwhile, monolayer excitons are limited by their intrinsic band structure, resulting in lacking electrical tunability. In contrast, interlayer excitons are electrically tunable, and external electric fields can adjust the dipole strength and exciton-photon interaction, making bilayer devices advantageous for dynamic modulation and integrated photonics applications.

To realize interlayer exciton lasing, Paik et al. used a rotationally aligned WSe<sub>2</sub>-MoSe<sub>2</sub> heterobilayer integrated with a SiN grating resonator (Figure 7a, left panel) [104]. This heterobilayer served as the gain medium, where interlayer excitons formed by electrons and holes in different monolayers enabled lasing. The alignment created a direct bandgap between the K valleys of the two monolayers, enhancing oscillator strength and efficient carrier transfer [132]. The resonator was designed to match exciton resonance, supporting cavity modes overlapping with the heterobilayer and providing spatial coherence [133]. Powerdependent PL measurements showed a linear increase in emission intensity above the threshold, confirming the onset of stimulated emission (Figure 4a, middle panel). Coherence measurements using a Michelson interferometer confirmed spatial coherence across the emission region (Figure 7a, right panel). Compared to monolayer exciton lasers, this system benefits from electrically tunable dipole interactions, robust valley polarization, and efficient population inversion [132], [134]-[136].

Unlike many interlayer exciton lasers requiring cryogenic temperatures [104], [111], Liu et al. demonstrated room-temperature lasing by integrating a MoS<sub>2</sub>/WSe<sub>2</sub> heterobilayer with a PCC in 2019 (Figure 7b, left panel) [103]. The interlayer excitons emitted in the infrared range (1,122.5 nm), making them compatible with the larger bandgap of silicon (Figure 7b, middle panel). The lasing threshold was approximately 33 mW (Figure 7b, right panel), and the longer lifetime of interlayer excitons allowed for lasing with lower Q-factors, suitable for practical integrated photonic devices [137], [138].

Moiré excitons also play a significant role in interlayer systems. These excitons are formed when two slightly misaligned 2D vdW materials create a moiré superlattice, providing periodic confinement potential [84], [86], [139]-[141]. Qian et al. demonstrated lasing from moiré excitons in a WSe<sub>2</sub>-MoSe<sub>2</sub> heterobilayer encapsulated in hBN and coupled with a high-O PCC (Figure 7c, left panel) [111]. Strong coupling between the cavity mode and excitons was observed, evidenced by a linear Zeeman shift under an applied magnetic field and linewidth narrowing above the lasing threshold (Figure 7c, middle panel and right panel), indicating increased coherence. These results highlight the tunability of interlayer exciton-cavity coupling, opening possibilities for quantum light sources and nanophotonic devices [142].

#### 3.3 2D vdW materials lasers without external cavities

The previously discussed 2D semiconductor lasers present benefits such as small size, low lasing thresholds, and tunable emission. However, they have the drawbacks of limited controllability, high optical losses on silicon substrates, and the complexity of fabricating external optical cavities. To reduce the production cost of on-chip integrated laser devices, simpler and more efficient large-scale manufacturing processes are crucial. In contrast, InSe demonstrates excellent compatibility with silicon and the ability to act as both the gain medium and the optical resonator [143]-[147], achieving lasing without the need for external optical cavities. This unique capability makes InSe a highly promising, cost-effective solution for integrated on-chip lasers.

In 2021, Li et al. mechanically exfoliated InSe microflakes of varying thicknesses and used optical pumping to achieve room-temperature near-infrared lasing [29]. InSe, a vdW crystal with covalently bonded Se-In-In-Se layers was exfoliated to form smooth surfaces (Figure 8a, left panel). Power-dependent PL spectra of InSe microflakes (Figure 8a, right panel) showed a transition from SE to lasing, with two peaks at 995 nm (X-peak, attributed to exciton recombination) and 1,027 nm (P-band, attributed to exciton-exciton scattering) [144]. At higher excitation power (0.62 mJ/cm<sup>2</sup>), multiple narrow lasing peaks appeared above the P-band with a free spectral range of ~3.38 nm and FWHM of 1.02 nm. Laser-printed microdisks (30 µm diameter) had reduced thresholds (~0.53 mJ/cm<sup>2</sup>) compared to pristine microflakes, with

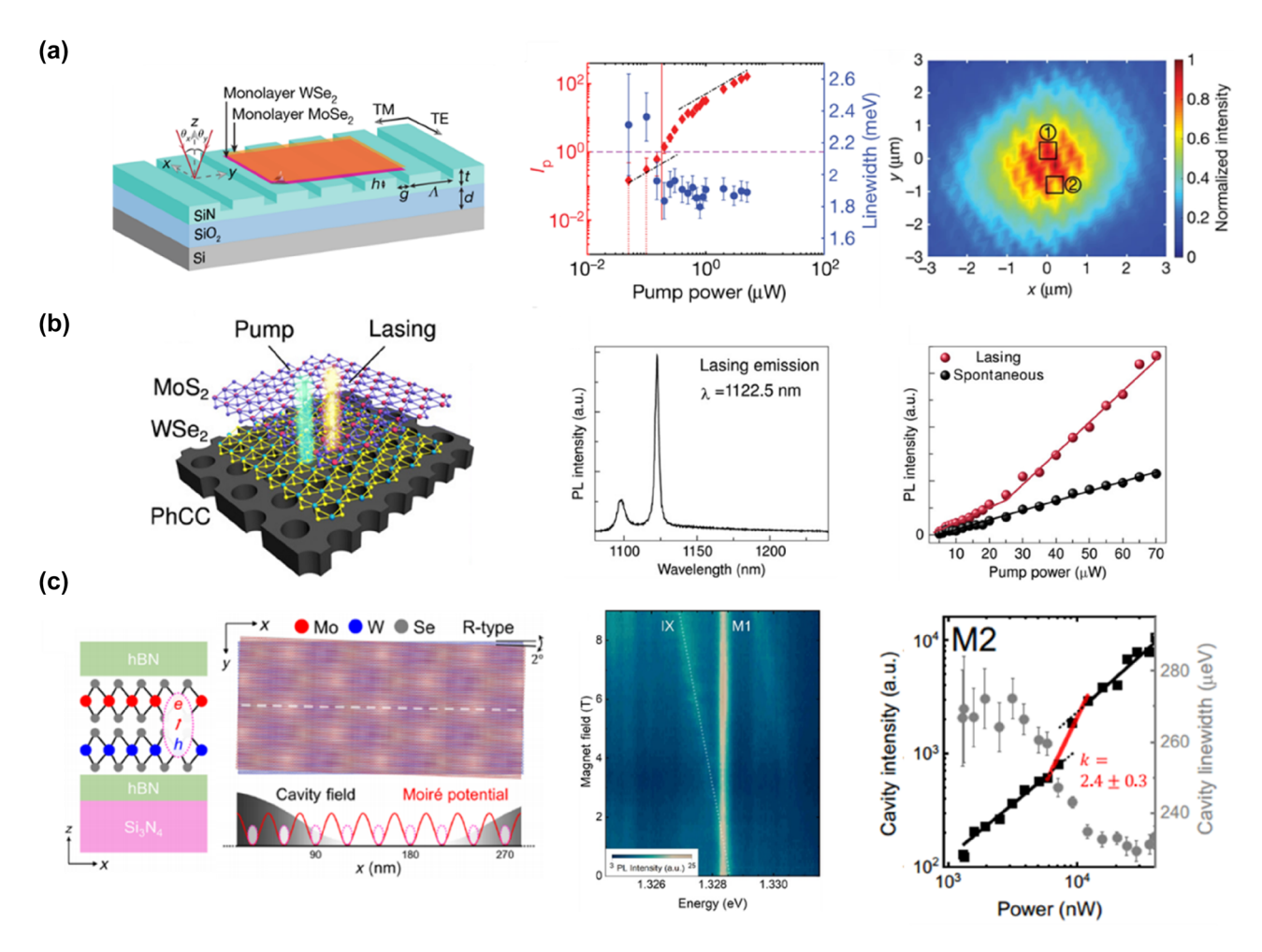
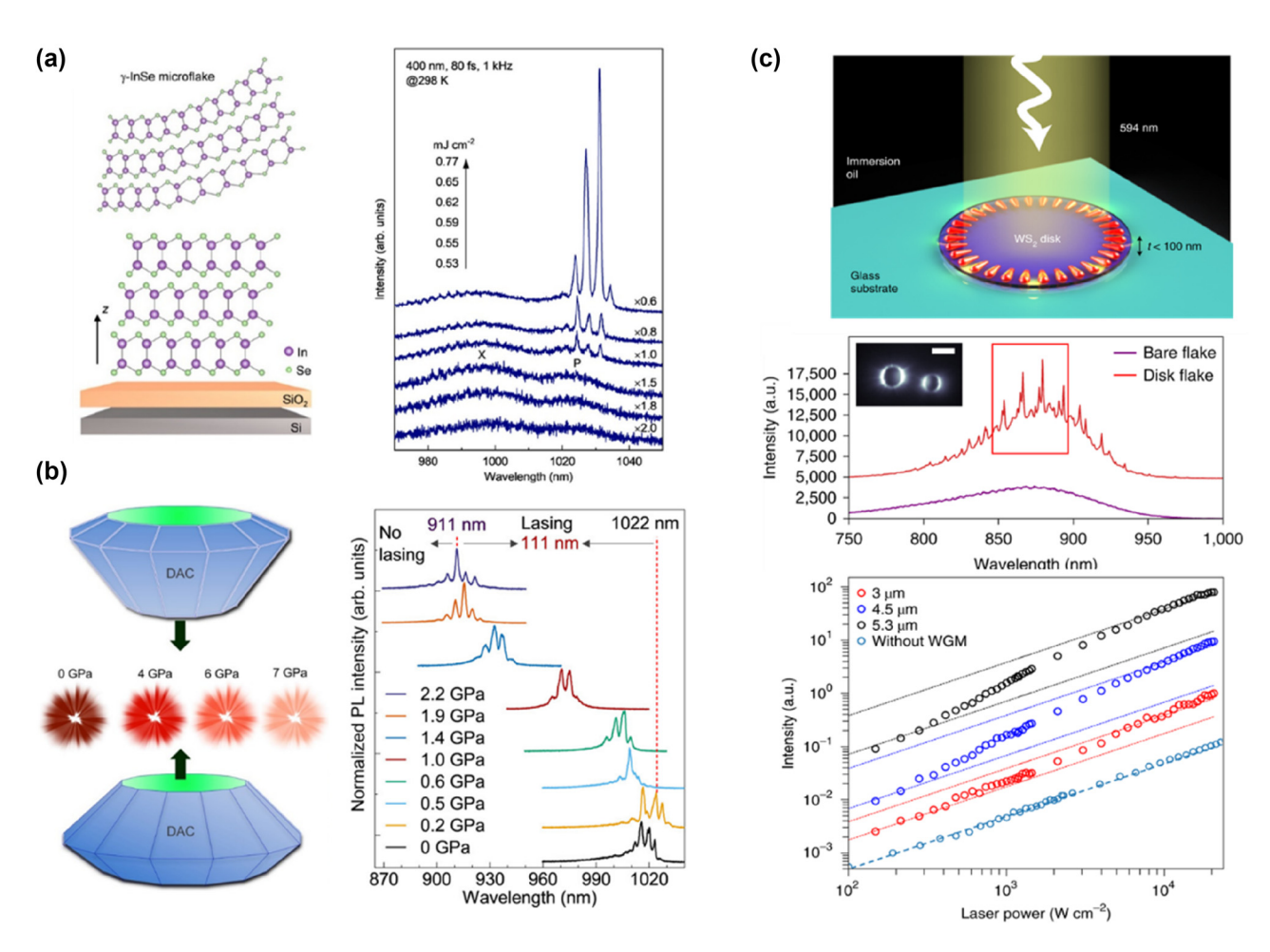


Figure 7: Three distinct cavity structures for TMD-based interlayer exciton lasers. (a) Left panel: the schematic of a heterobilayer WSe<sub>2</sub> – MoSe<sub>2</sub> laser device integrated with a SiN grating cavity. Middle panel: a plot of the photon occupancy and linewidth of the TE-polarized emission as a function of pump power. The photon occupancy (red dots) shows a superlinear increase at the threshold (vertical red line), while the linewidth (blue dots) narrows, indicating the onset of lasing. Right panel: the interference pattern observed in the Michelson interferometer setup at a power above the lasing threshold (20 μW). Reproduced from ref. [104]. Copyright 2019, Springer Nature. (b) Left panel: schematic of a nanocavity laser device using a MoS<sub>2</sub>/WSe<sub>2</sub> heterostructure as the gain medium. Middle panel: the emission spectrum of the cavity lasing mode at 5 K with a CW pump power of 190 mW. The lasing action is observed at approximately 1,122.5 nm with a linewidth of ~2.7 nm. Right panel: the L−L curve for the laser. The cavity mode intensity (red dots) exhibits a clear kink, typical of lasing onset, while the background emission (black dots) remains linear. Reproduced from ref. [103]. Copyright 2019, AAAS. (c) Left panel: schematic of the MoSe<sub>2</sub>/WSe<sub>2</sub> heterobilayer integrated with a nanocavity and encapsulated by hexagonal boron nitride (hBN). The right side displays the electric field distribution in the nanocavity. Middle panel: PL spectrum for the MoSe<sub>2</sub>/WSe<sub>2</sub> heterobilayer coupled with a nanocavity, recorded under low excitation power at 88 nW and in the presence of a magnetic field. Right panel: power-dependent behavior of the PL intensity and linewidth of cavity mode M2, indicating the transition to lasing. Reproduced from ref. [111]. Copyright 2024, AAAS.

emission coupled out from the microdisk's edge, indicating in-plane WGM resonance [148]. These results highlight InSe's potential for near-infrared on-chip lasers for imaging, sensing, and optical interconnects [89], [138], [149], [150]. To expand InSe's emission characteristics, Zhao et al. applied hydrostatic pressure, achieving broad spectral tuning (Figure 8b) and demonstrating the flexibility of InSe for tunable near-infrared microlasers [151].

In studies of 2D TMD lasers, monolayer materials are often used due to their direct bandgap, which allows efficient radiative recombination without requiring phonons [1], [3], [10]. However, large-scale fabrication of monolayers is challenging. Achieving lasing in nonmonolayer TMDs with indirect bandgaps would simplify mass production of 2D semiconductor lasers. In 2022, Sung et al. demonstrated that an ultra-thin WS2 disk (~50 nm) supports WGMs and provides sufficient optical gain for lasing without an external cavity (Figure 8c, top panel) [112]. The WS<sub>2</sub> disk, fabricated via mechanical exfoliation and reactive ion etching, served as both gain



**Figure 8:** Laser emission and modulation of vdW materials without external optical cavities. (a) Left panel: schematic of mechanically exfoliated γ-InSe microflake placed on a SiO<sub>2</sub>/Si substrate. Right panel: the power-dependent PL spectra of a single InSe microflake at 298 K under femtosecond pulse laser excitation (400 nm, 1 kHz, 80 fs). Reproduced from ref. [29]. Copyright 2021, American Chemical Society. (b) Left panel: schematic of a diamond anvil cell used for high-pressure experiments. Right panel: the laser PL spectra of a single γ-InSe platelet under hydrostatic pressure ranging from 0 to 2.2 GPa. During the application of pressure, the laser emission's central wavelength shifts from 1,022 nm to 911 nm. Reproduced from ref. [151]. Copyright 2022, American Chemical Society. (c) Top panel: 3D schematic image of an optically pumped WS<sub>2</sub> disk nanolaser. Middle panel: the PL spectrum for a patterned WS<sub>2</sub> disk, revealing multiple WGM peaks on top of a broad emission background from the indirect bandgap transition. The inset displays an emission image of the WS<sub>2</sub> disk at the lasing wavelength, above the lasing threshold, which shows the light emission from the disk edge where the WGMs are formed. Bottom panel: the L–L curves of WS<sub>2</sub> microdisks with different diameters. The green data indicate the SE from the indirect bandgap without coupling to WGMs, while the WGM-associated lasing action shows a nonlinear increase in intensity, indicating lasing behavior. Reproduced from ref. [112]. Copyright 2022, Springer Nature.

medium and resonant cavity. Its emission spectrum showed sharp WGM peaks over a broad indirect-bandgap background (Figure 8c, middle panel). With increased pumping power, the WGM peaks transitioned from SE to amplified spontaneous emission (ASE) and eventually to lasing, forming an "S-shape" in the L–L curve (Figure 8c, bottom panel). The lasing relied on phonon-assisted emission through a three-level system. This work challenges the belief that indirect-bandgap materials are unsuitable for lasing and underscores their potential for optical and optoelectronic applications.

#### 3.4 A special type: emission from EP

The above discussion focused on exciton lasers in 2D semiconductor materials, which rely on stimulated emission of photons to generate coherent light, requiring a high density of photons to achieve population inversion. Next, we introduce a special and efficient form of light-matter interaction – EPs. EPs are hybrid quasi-particles formed through the strong coupling between photons and excitons, combining the light-like properties of photons with the matter-like properties of excitons [152]. EPs are unique in that they combine the low effective mass of photons with the strong interaction properties of excitons. Due to the photonic component, polaritons can propagate with an extremely low effective mass [153], resulting in high mobility, making them ideal for fast-response optical devices. Meanwhile, the excitonic component imparts strong nonlinearity [154], which makes EPs particularly advantageous for achieving significant nonlinear optical effects at low power. This strong light-matter coupling results in Rabi splitting, leading to the formation of two polariton branches - the upper polariton branch (UPB) and the lower polariton branch (LPB) - characterized by distinct energy levels and hybrid properties. In the dispersion relation, an anticrossing phenomenon between exciton and photon energies can be observed from angle-resolved spectroscopy, which demonstrates the occurrence of strong coupling between the two, leading to the formation of EPs [155].

#### 3.5 Emission from EP with external cavities

Zhang et al. developed a novel strong coupling system combining one-dimensional (1D) photonic crystals (PCs) with monolayer TMDs like WSe<sub>2</sub> and WS<sub>2</sub> (Figure 9a, top panel) [133]. The SiN PCs coupled with the monolayer TMDs provided a compact platform for strong coupling at room temperature, with observed mode anticrossing (Figure 9a, bottom panel) and tunable Fano resonances. Adjusting PC parameters allowed flexible control over polariton modes, suggesting applications in polariton lasers, amplifiers, and switches [156]-[160].

As bosons, EPs have the ability to undergo BEC under appropriate conditions. The process of BEC can be summarized as generation of EPs, cooling and thermalization, stimulated scattering leading to accumulation in the ground state, and finally formation of a macroscopic coherent state.

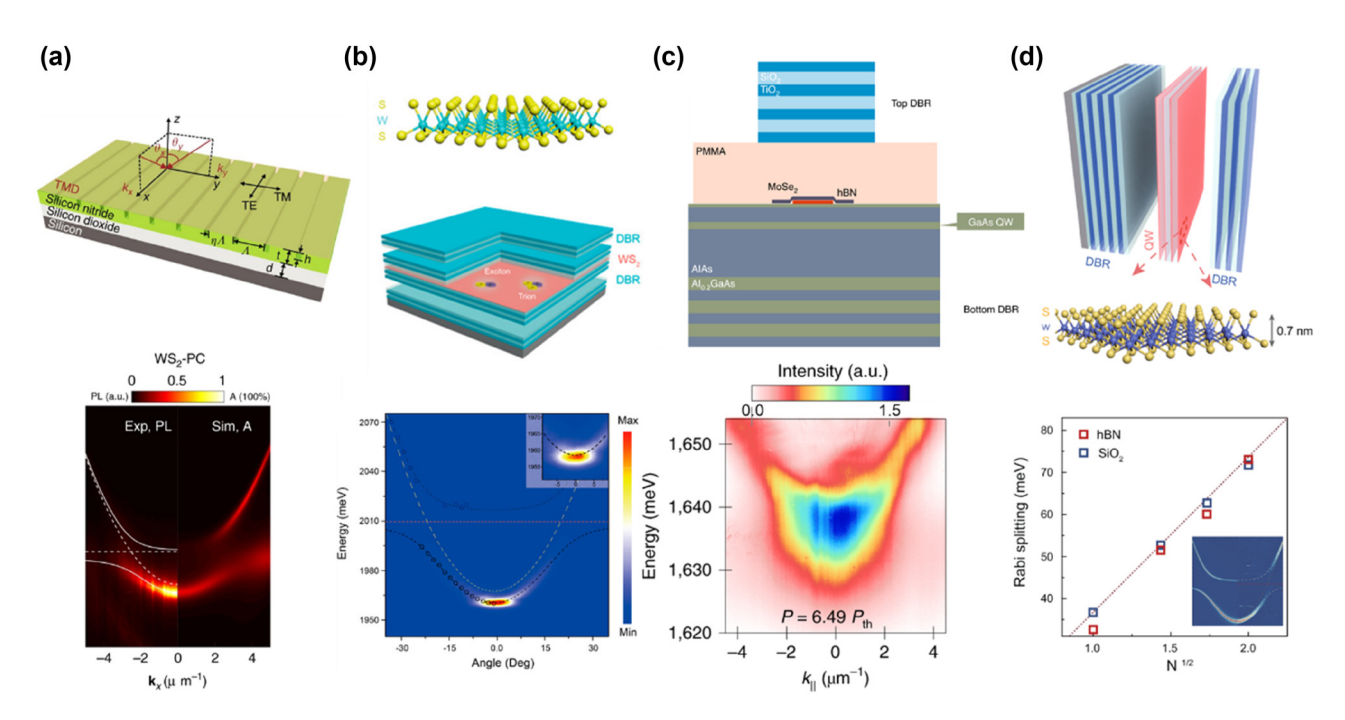


Figure 9: Emission from EP with external cavities. (a) Top panel: schematic of the structure integrating a monolayer TMD, such as WSe<sub>2</sub> or WS<sub>2</sub>, with a 1D photonic crystal (PC). Bottom panel: angle-resolved PL map and corresponding simulated absorption spectra of the WS<sub>2</sub>-PC integrated device at room temperature. Reproduced from ref. [133]. Copyright 2018, Springer Nature. (b) Top panel: schematic of the structure integrating a monolayer  $WS_2$  into an all-dielectric  $\lambda/2$  planar microcavity. Bottom panel: the angle-resolved PL map of the  $WS_2$  microcavity above the lasing threshold. The inset provides a zoomed-in view of the ground state, showing that the intense ground state emission is associated with the formation of a localized polariton condensate in a spatial trap. Reproduced from ref. [163]. Copyright 2021, American Chemical Society. (c) Top panel: schematic of the sample structure where a monolayer MoSe, is embedded in a hybrid III/V dielectric microcavity. The structure consists of DBR, hBN, and polymethyl methacrylate spacer layers. Bottom panel: the dispersion relation map of EP condensation at pump power above the threshold ( $P = 6.49 P_{tb}$ ). Reproduced from ref. [169]. Copyright 2023, Springer Nature. (d) Top panel: schematic diagram of the WS<sub>2</sub> superlattice embedded in a full dielectric planar microcavity. Bottom panel: the relationship between the Rabi splitting and the square root of the number of layers, comparing the experimental results using hBN (red) and SiO<sub>2</sub> (blue) as insulators. It is observed that the Rabi splitting increases with the square root of the number of layers, demonstrating the enhancement of coupling strength in the multilayer WS<sub>2</sub> superlattice. The inset shows the angle-resolved reflectivity map for a microcavity containing a WS<sub>2</sub> superlattice with two layers. Reproduced from ref. [170]. Copyright 2023, Springer Nature.

In this condensed state, the coherence of polaritons results in the emission of coherent light, which manifests as ultralow threshold lasing [153]-[155], [161]. However, traditional polariton systems, such as those based on III-V materials (e.g., GaAs [162]), typically require cryogenic temperatures to achieve condensation. Zhao et al. demonstrated roomtemperature polariton condensation in a monolayer WS<sub>2</sub> microcavity using a  $\lambda/2$  structure embedded between DBRs (Figure 9b, top panel) [163]. The above-threshold angleresolved PL map displays a sharp and intense peak near the ground state, which does not fully follow the LPB dispersion indicated by the black dashed line but instead appears delocalized in momentum space, suggesting the formation of a localized polariton condensate (Figure 9b, bottom panel). Meanwhile, spatial traps increased local polariton density, promoting condensation. This work suggests potential in valleytronics, quantum information, and low-power coherent light sources [156], [164]-[168]. Solanas et al. reported bosonic condensation of EPs in a microcavity loaded with a monolayer of MoSe<sub>2</sub> at cryogenic temperatures (Figure 9c) [169]. Under an external magnetic field, valley polarization was observed, with an energy splitting between K and K' polaritons. This demonstrates potential for valleytronic optoelectronic devices.

TMD materials can be stacked to form artificial vdW superlattices because the weak vdW forces between layers allow precise control over the stacking sequence and alignment, providing unique opportunities to manipulate light-matter interactions. Gaining insight into these interactions enables precise control over quasiparticles that merge the properties of light and matter. Zhao et al. demonstrated control of coupling strength by embedding multiple WS<sub>2</sub> monolayers in a planar microcavity (Figure 9d, top panel) [170]. Increasing the number of layers enhanced vacuum Rabi splitting from 36 meV to 72 meV (Figure 9d, bottom panel), improving EP stability. Additionally, phase space filling effects and long-lived dark excitons were observed, paving the way for low-power optical circuits and applications in photonics, quantum information, and integrated systems [171].

#### 3.6 Emission from EP without external cavities

As stated above, EPs have traditionally been realized using external optical cavities such as Fabry-Pérot resonators, DBRs, or plasmonic nanostructures. These cavity-based systems enhance exciton-photon interactions by providing strong optical confinement, resulting in large Rabi splitting and enabling applications in polariton lasing, quantum

optics, and nonlinear photonics. However, such architectures come with practical limitations, including fabrication complexity, integration challenges, and scalability issues, particularly for ultra-thin, atomically layered materials like TMDs. Recently, a new class of EPs has emerged, which does not require external cavities. Instead, these self-hybridized EPs rely on intrinsic optical resonances within the TMD itself or engineered photonic structures such as gratings [172] and PCs [173]. By leveraging the high refractive index, strong excitonic response, and in-plane light confinement of TMD multilayers, researchers have demonstrated cavityfree EPs in bare WS2 layers [174] and WS2-based nanostructures [172], [173]. These advancements pave the way for compact, highly tunable polaritonic devices that can operate at room temperature without the constraints of external cavity fabrication. The following discussion explores three studies that demonstrate EP emission in cavity-free systems.

In 2022, Shin et al. provided direct experimental confirmation of self-hybridized EPs in bare WS<sub>2</sub> multilayers, proving that strong exciton-photon coupling can occur without external optical cavities [174]. Using evanescent field coupling (Figure 10a), the authors investigated the dispersion, tunability, and valley polarization of these guided EPs. Their findings reveal clear anticrossing behavior near the exciton resonance (Figure 10b), with Rabi splitting energy varying based on layer thickness, confirming thickness-dependent strong coupling effects. Additionally, they demonstrated that the guided EPs retain valley polarization up to 0.2 at room temperature, making them promising candidates for valleytronic applications. Furthermore, they showed that the EP dispersion can be continuously tuned via excitation power, highlighting the high degree of control and adaptability of these self-hybridized polaritons. These results provide strong evidence that bare WS<sub>2</sub> layers can support nonradiative EPs, opening new possibilities for integrated nanophotonic and valleytronic devices.

Cho et al. addressed the challenge of far-field detection of guided EPs by integrating a 1D PC (grating structure) into WS<sub>2</sub> multilayers (Figure 10c) [172]. While guided EPs normally exist as nonradiative modes confined within the WS<sub>2</sub> layer, the periodic grating structure enables momentum matching, allowing them to be coupled into the far field for optical measurement. Through angle-resolved reflectance and PL spectroscopy (Figure 10d), the authors confirm the formation of guided-mode resonances in WS2 gratings as thin as 10 nm. They also demonstrate that strong excitonic resonances in WS2 naturally lead to guided EP formation, and the grating facilitates efficient coupling of these modes into free space. This work bridges the gap between nonradiative polariton physics and practical photonic

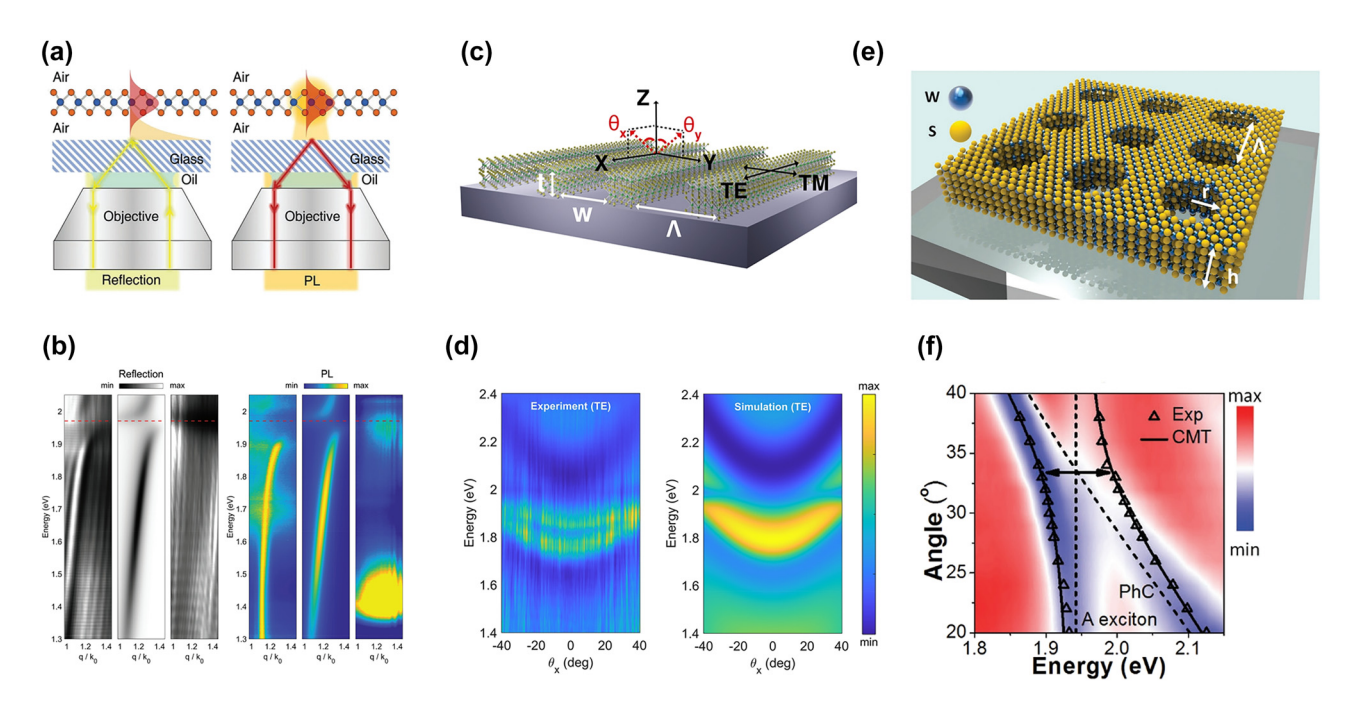


Figure 10: Emission from EP without external cavities. (a) Schematic of evanescent field coupling. Left panel: white-light reflection measurements probe photon modes in suspended WS<sub>2</sub>. Right panel: PL measurement under 594 nm laser excitation. (b) Angle-resolved reflection and PL spectra. Left (right) panel: angle-resolved reflection (PL) spectra for suspended WS, layers (left), simulation (middle), and nonsuspended WS, layers (right). A clear anticrossing behavior is visible, confirming strong exciton-photon coupling, leading to the formation of EP branches. Panel (a-b): reproduced from ref. [174]. Copyright 2022, Wiley-VCH. (c) Schematic of the 1D WS<sub>2</sub> grating structure. (d) Left (right) panel: experimentally measured (theoretical) TE-polarized angle-resolved reflection spectrum in x-direction. A strong anticrossing behavior appears near 1.97 eV (exciton resonance). Panel (c-d): reproduced from ref. [172]. Copyright 2023, De Gruyter. (e) The structural design of an ultrathin WS<sub>2</sub> PC. A patterned square array of air holes is fabricated in the layered WS<sub>2</sub> on a glass substrate. (f) The experimental angle-resolved transmission spectrum of the WS<sub>2</sub> PC. Two clear polariton branches are observed, confirming strong exciton-photon coupling. Panel (e-f): reproduced from ref. [173]. Copyright 2020, Wiley-VCH.

applications, paving the way for scalable, on-chip excitonpolaritonic devices using WS<sub>2</sub>-based nanostructures.

Zhang et al. demonstrated a WS2 PC as a self-resonant polariton system, eliminating the need for external cavities (Figure 10e) [173]. The 12 nm-thick WS<sub>2</sub> PC supports intrinsic optical resonances, leading to anticrossing at 1.97 eV and a Rabi splitting of ~100 meV (Figure 10f). This design achieves deep subwavelength light confinement, offering a new approach for ultra-thin polaritonic and quantum photonic devices.

These three works collectively demonstrate the feasibility and advantages of cavity-free EPs, establishing new methods to generate, manipulate, and observe polaritonic states, offering new possibilities for scalable nanophotonic devices, integrated valleytronic systems, and ultra-compact quantum photonic technologies.

In addition to the research on polaritons in the aforementioned TMD materials, CrSBr, as a novel 2D layered magnetic semiconductor, has attracted widespread attention recently due to its unique structural, electronic, magnetic, and optical properties. The crystal structure of CrSBr comprises chromium sulfide double layers flanked on both

sides by anionic bromide layers, all separated by vdW gaps (top image of Figure 11a) [175]. This configuration allows for straightforward mechanical exfoliation down to monolayer or few-layer thicknesses. Each chromium ion resides in a distorted octahedral coordination environment formed by four sulfur atoms and two bromine atoms, which contributes to the material's electronic and magnetic anisotropy. CrSBr exhibits A-type antiferromagnetic order below its Neél temperature of 132 K. In this magnetic state, spins align ferromagnetically within each vdW layer and antiferromagnetically between adjacent layers (bottom image of Figure 11a) [176], [177]. This material shows strong triaxial magnetocrystalline anisotropy, with the b-axis serving as the easy magnetic axis, the a-axis as the intermediate magnetic axis, and the c-axis being the hard magnetic axis. When a magnetic field is applied along the b-axis, a sharp transition to magnetic saturation occurs, which is consistent with a spin-flip transition due to large magnetocrystalline anisotropy energy [176]-[178]. In addition to magnetic anisotropy, CrSBr exhibits significant optical anisotropy, including PL that exhibits strong polarization dependence. The PL intensity is strongest when

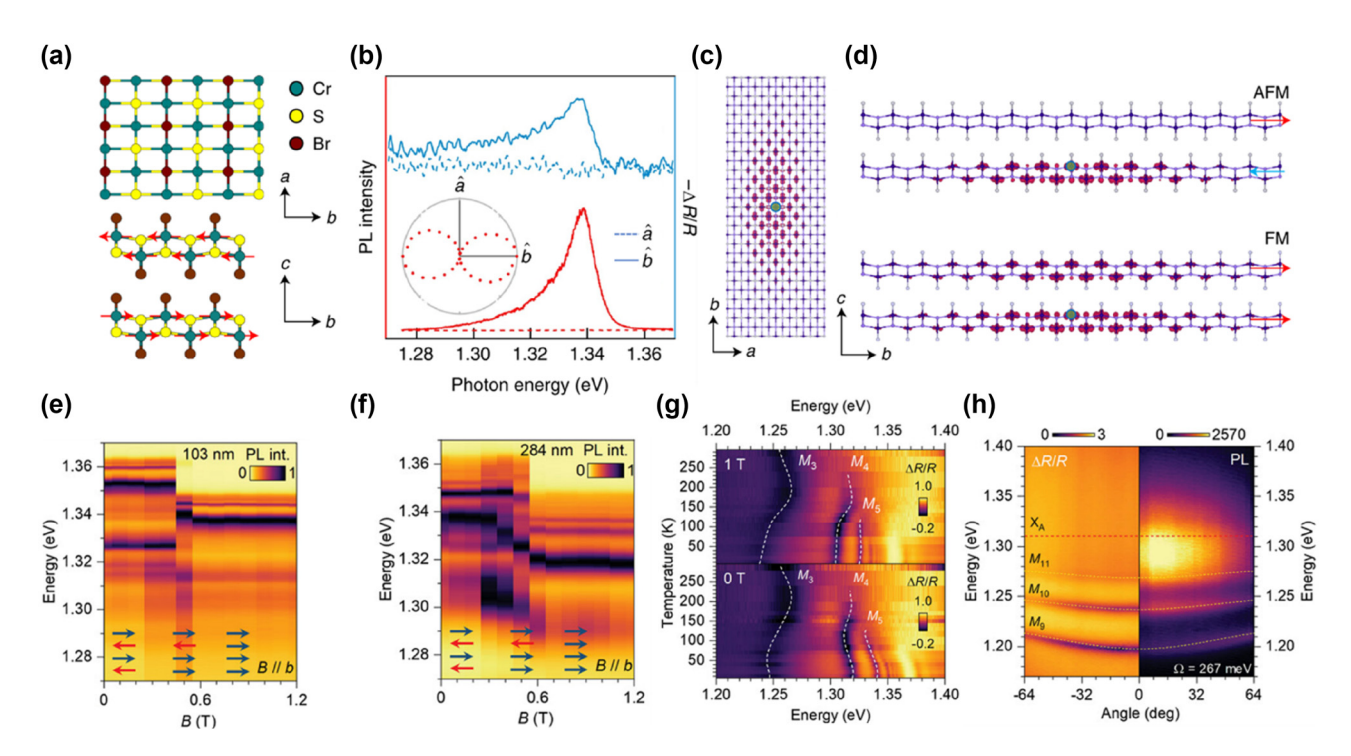


**Figure 11:** The properties and special EP characteristics of a novel 2D magnetic vdW material, chromium sulfide bromide (CrSBr). (a) The crystal and magnetic structures of CrSBr. The top image is a top view of a single CrSBr layer, depicting the 2D layered structure of the material, while the bottom image is a side view of a bilayer CrSBr, where red arrows represent the interlayer antiferromagnetic (AFM) order. (b) The differential reflectance spectra (blue) and PL spectra (red) of bilayer CrSBr with light polarized along the *b*-axis (solid lines) and *a*-axis (dashed lines). (c) Top view of the real-space wavefunction of the lowest-energy exciton in CrSBr bilayer. (d) The side view of the exciton wavefunction in the AFM bilayer (top) and ferromagnetic (FM) bilayer (bottom) state. Panel (a – d): reproduced from ref. [179]. Copyright 2021, Springer Nature. (e, f) The normalized 2D colored PL spectra of the 103 nm-thick (e) and 284 nm-thick (f) CrSBr crystals at 10 K under a magnetic field (*B*) ranging from 0 to 1.2 T. (g) The 2D reflectance spectra of the 354 nm-thick CrSBr crystal under 0 T (bottom panel) and 1 T (top panel) magnetic fields. (h) Angle-resolved reflectance and angle-resolved PL map at 298 K of the 1,260 nm-thick CrSBr crystal. Panel (e–h): reproduced from ref. [31]. Copyright 2024, Wiley-VCH.

the incident light is polarized along the b-axis and weakest when polarized along the a-axis (Figure 11b). This indicates that the excitonic wavefunction is more delocalized along the b-axis than the a-axis (Figure 11c), in agreement with the anisotropic band structure [179]. In the AFM state, interlayer hybridization is suppressed due to antialigned spins, whereas in the FM state, electronic wavefunctions can couple between layers (Figure 11d), resulting in band splitting and a reduction in the bandgap. These computational results align well with the experimentally observed exciton redshift, highlighting the crucial role of magnetic ordering in interlayer electronic coupling [179]. The 2D nature and high stability of CrSBr make it an ideal platform for studying low-dimensional quantum physics and correlated electronic phenomena, including research into magnetic correlations at low temperatures [180], EPs [31], [181], [182], and other complex physical phenomena.

CrSBr flakes with sufficient thickness form microcavities, enabling strong exciton—photon interactions along the *b*-axis, leading to self-hybridized EPs [181], [182]. Li et al.

demonstrated stable EP behavior in CrSBr crystals, investigating the effects of thickness, magnetic field, and temperature [31]. Figures 10f and 11e show PL spectra of CrSBr crystals (108 nm and 203 nm) at 10 K under magnetic fields. At 0.5 T, a redshift occurs, indicating a transition from AFM to FM. Figure 11g shows a redshift in EP energy at 1 T, which decreases with increasing temperature. Figure 11h shows the angle-resolved reflectance and angle-resolved PL imaging for a much thicker CrSBr crystal (1,260 nm) at room temperature (298 K), indicating a Rabi splitting energy of 267 meV, confirming ultrastrong coupling. CrSBr's magnetic tunability and strong coupling at room temperature make it ideal for photonic devices like tunable filters, photodetectors, and light sources, with promising near-infrared applications.

#### 4 SPE from 2D vdW materials

In recent years, quantum photonics has brought transformative advancements across multiple fields, including

secure communication [183], computation [184], [185], and sensing [186]. Single-photon sources play a vital role in this field by enabling precise control over light-matter interactions at the nanoscale. For 2D SPE, three key aspects (emission origin, defect engineering, and rational design) play crucial roles in optimizing the efficiency and stability of quantum light sources.

Emission origin—In the simplest case, an SPE can be modeled as a two-level system, defined by its transition energy and dipole matrix element, as mentioned above. SPE in 2D materials originates from quantum-confined excitons that become trapped in localized defect states or strain-induced potential wells. The fundamental requirement for SPE is that only one exciton can occupy the localized state at a time, preventing multiphoton emission. Defect-state emission occurs when atomic-scale vacancies or substitutional atoms introduce deep mid-gap states, trapping excitons at these defect sites where they undergo radiative recombination, emitting single photons. A notable example is nitrogen vacancies in hBN, which enable roomtemperature SPE due to their deeply localized states [17]. Strain-induced exciton localization, on the other hand, modifies the local bandgap, forming potential wells that capture excitons. These localized excitons recombine to produce narrow and stable SPE peaks. A prominent example is strain-induced quantum dots (QDs) in WSe2, which serve as efficient single-photon sources. Lastly, in twisted bilayers, such as MoSe<sub>2</sub>/WSe<sub>2</sub> heterobilayers [140], periodic Moiré superlattices create spatially confined exciton potential minima. These potential traps localize excitons, facilitating deterministic SPE, making them highly attractive for quantum photonics applications.

Defect engineering—Defect engineering in 2D singlephoton emitters involves the intentional creation, modification, and control of atomic-scale defects to tailor optical and electronic properties, enabling SPE. In this process, defects introduce localized electronic states within the material's bandgap, trapping excitons and ensuring that photons are emitted one at a time, a crucial feature for quantum applications. Various methods have been developed to create and control these defects in TMDs and hBN. Ion beam irradiation, using focused helium or neon ion beams, displaces atoms from the lattice to form vacancies, which act as exciton traps in materials like MoS<sub>2</sub> [187] and WSe<sub>2</sub> [188]. Similarly, high-energy electron beam irradiation modifies atomic arrangements, generating stable defect sites such as nitrogen and boron vacancies in hBN, known for their robust room-temperature quantum emission [189], [190]. Chemical functionalization and annealing provide another avenue for defect control, where selective exposure to

oxidizing or reducing agents modifies defect states, and thermal annealing either activates or passivates these states to enhance emission stability [191]. Additionally, strain engineering, achieved through nanopillars or wrinkled substrates, alters the local band structure, forming quantumdot-like potential wells that localize excitons and enhance SPE. In twisted bilayers of TMDs, Moiré superlattices naturally create periodic exciton potential traps, leading to deterministic SPE [140]. These advanced defect engineering techniques enable precise control over quantum emitters, paving the way for scalable and high-purity single-photon sources essential for quantum communication, computation, and sensing applications.

Rational design—To engineer high-performance SPEs, several strategies have been employed. Strain and electric field tuning have been demonstrated to dynamically modulate emission wavelengths, while gate-tunable heterostructures, such as graphene/hBN [192], enable controlled chargestate switching for enhanced emission control. Coupling these emitters to optical cavities significantly boosts their brightness and extraction efficiency [193]-[195]. Additionally, charge-state control through electrical gating allows for on-demand switching of emission, improving stability and robustness [196]. For large-scale applications, deterministic positioning of SPEs is crucial, and plasmonic array offers a promising approach to creating ordered SPE arrays for integrated quantum photonic networks [197].

Effective single-photon sources must exhibit high brightness, purity, and indistinguishability to support quantum technologies like secure quantum communication and quantum computing. Brightness quantifies the probability of emitting a single photon upon excitation, purity refers to the source's ability to emit only one photon per event, and indistinguishability ensures that each photon remains consistent across different degrees of freedom [198]. Each of these factors is essential to applications requiring interference, like quantum computing, where photon consistency is crucial for multiphoton interactions [199], [200]. Therefore, the selection of materials for single-photon sources requires multifaceted consideration. While traditional platforms like QDs [201]-[206] and nitrogen-vacancy [207]-[210] centers in diamonds have set benchmarks, novel 2D vdW materials such as TMDs and hBN are rapidly gaining attention.

TMDs are particularly notable for their strong electron-hole binding energy, which supports SPE through excitons trapped by localized defects or strain. Since the demonstration of SPE from TMDs in 2015 [18], [19], [211]–[213], numerous methods have emerged to enhance their emission efficiency. For instance, coupling TMDs to plasmonic nanostructures like GaP nano-antennas has achieved brightness levels near 0.86 and quantum efficiency of approximately 80 % [214]. These modifications allow TMDs to produce bright, high-purity SPEs with relatively fast emission rates, making them suitable for low-temperature quantum information processing applications.

Due to the wide bandgap and remarkable resistance to decoherence, hBN enables stable SPE even at room temperature. The single-photon emitters in hBN, often linked to boron or nitrogen vacancies, are robust even under ambient conditions, making them an attractive candidate for quantum photonics [215]-[224].

One of the major challenges in single-photon source research is achieving tunability to ensure that the light source meets the demands of quantum applications while enhancing system stability and adaptability. In recent years, researchers have made significant advances in the tunability of single-photon sources, including strain tuning, electric field tuning, magnetic field tuning, and cavity coupling.

As shown in Figure 12a, Branny et al. used nanoscale strain engineering to create local strain perturbations in monolayer and bilayer WSe<sub>2</sub> [225]. They placed lithographically patterned nanopillars under atomically thin WSe<sub>2</sub> flakes, which induced significant localized elastic strain at the nanopillar sites. This strain modified the band-gap of the semiconductor, funneling excitons to these smaller bandgap regions, leading to the formation of highly pure single photon-emitting quantum emitters. The use of nanopillars enabled the precise positioning of these quantum emitters. By adjusting the nanopillar dimensions, they improved both the yield of emitter formation and their positioning accuracy. This strain-based control method is well-suited for creating scalable and structured arrays of single-photon emitters.

In 2019, Iff et al. demonstrated a hybrid structure combining a 2D semiconductor and a piezoelectric device to control the emission energy of single-photon emitters in WSe<sub>2</sub> monolayers (Figure 12b) [226]. Specifically, they used

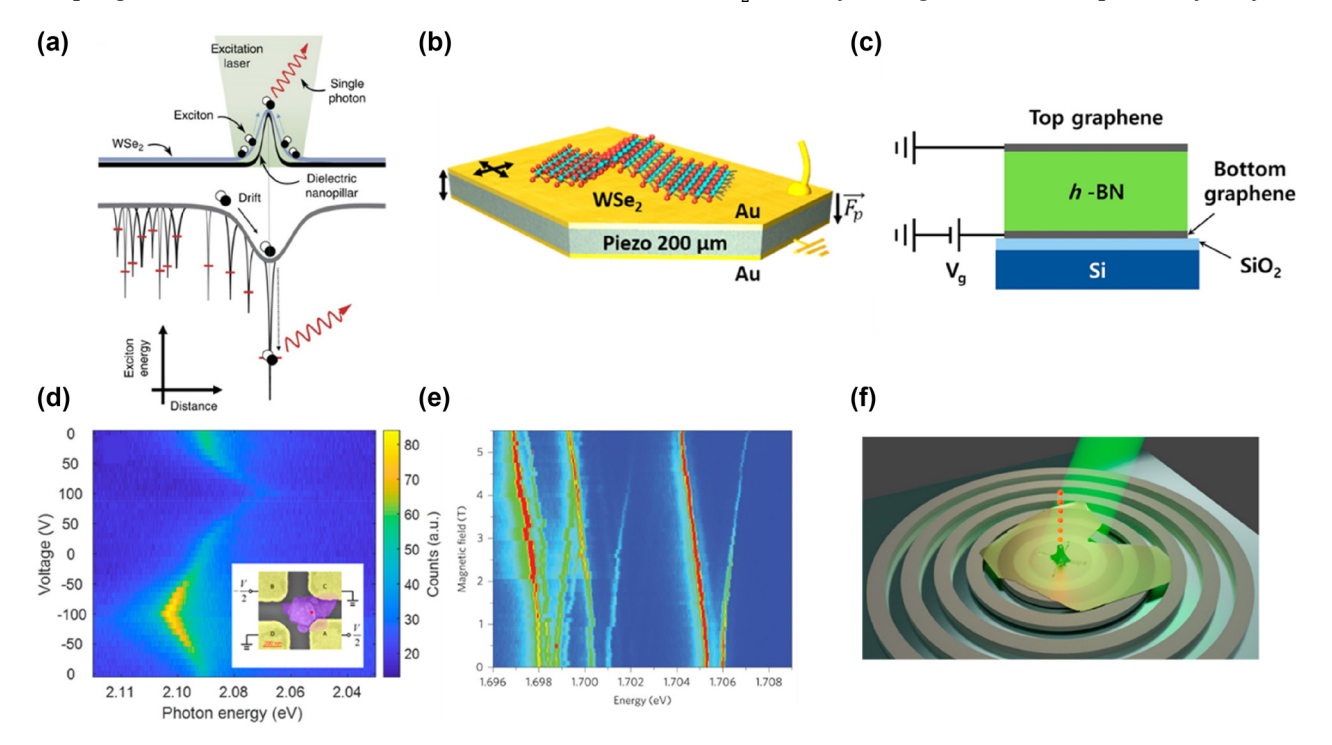


Figure 12: Different modulation methods of SPE from 2D vdW materials. (a) The concept of achieving strain-induced quantum emitters in atomically thin WSe<sub>2</sub> using an array of nanopillars. The local biaxial strains modify the bandgap of WSe<sub>2</sub> and spatially modulate the potential landscape of the 2D excitons, leading to the efficient funneling of photoexcited excitons toward the lower energy states at the strain-tuned sites, eventually forming efficient single-photon quantum emitters. Reproduced from ref. [225]. Copyright 2017, Springer Nature. (b) Schematic of a hybrid 2D-semiconductorpiezoelectric actuator device with an integrated WSe, monolayer. Reproduced from ref. [226]. Copyright 2019, American Chemical Society. (c) The device schematic of multilayer hBN sandwiched between top and bottom few-layer graphene electrodes. This device is designed to tune the emission energy of single-photon emitters through the Stark effect by applying an out-of-plane electric field. Reproduced from ref. [232]. Copyright 2018, American Chemical Society. (d) The shift of the zero-phonon line PL spectrum's central wavelength of a single-photon emitter in hBN under different applied voltages. The inset shows the setup for applying voltage between electrodes A and B. Reproduced from ref. [233]. Copyright 2019, American Chemical Society. (e) The PL intensity plot of five single quantum emitters as a function of the applied magnetic field, ranging from 0 T to 5.5 T. Reproduced from ref. [19]. Copyright 2015, Springer Nature. (f) The design and characteristics of the Purcell-enhanced single-photon source based on a circular Bragg grating cavity. Reproduced from ref. [236]. Copyright 2021, American Chemical Society.

piezoelectric actuators to apply strain fields, allowing for the energy of localized excitons to be tuned by up to 18 meV. The strain was applied via an electric field across the sample, which consisted of a mechanically exfoliated WSe<sub>2</sub> monolayer transferred onto a piezoelectric plate. Using PL spectroscopy, the researchers observed both redshifts and blueshifts in emission energy under strain modulation. This study provides a new approach for creating energy-tunable single photon sources.

The emission energies of different emitters are often inhomogeneous, which poses a significant challenge for quantum information processing [227]-[229]. Therefore, a method to tune the emission energy of individual emitters is required. The Stark effect refers to the phenomenon in which the energy levels of electrons within atoms or molecules shift or split under the influence of an external electric field [230], which is an effective approach that enables the tuning of SPE energies through the application of an external electric field [231]. Noh et al. combined exfoliated hBN flakes with graphene to create heterostructures with top and bottom graphene electrodes (Figure 12c) [232]. Applying a voltage generated a vertical electric field to control defect centers in hBN, resulting in Stark-induced tuning of the emission with a maximum shift of 5.4 nm per GV/m. This work showed electric field control of hBN single-photon emitters. Xia et al. later designed a four-electrode nanodevice for more flexible electric field control, achieving a large Stark shift of 43 meV/(V/nm), the highest reported at room temperature [233]. Figure 12d shows the zero-phonon line PL intensity as a function of the applied voltage, with a Stark shift up to 31 meV, demonstrating reversible tuning of the single-photon emitter energy by the electric field.

Meanwhile, the emission characteristics of singlephoton sources can also be controlled by magnetic fields. He et al. introduced defect-localized excitons in WSe2 monolayers as single quantum emitters with narrow optical emission linewidths (~130 μeV), much narrower than delocalized valley excitons [19], [234]. These emitters exhibit two nondegenerate, linearly polarized transitions at zero magnetic field [235]. Applying a magnetic field causes the polarization to transition from linear to circular as it competes with electron-hole exchange interactions, leading to the Zeeman effect (Figure 12e). The magnetic field splits the energy levels of each emitter and controls the polarization state of emitted photons, enhancing the flexibility of singlephoton sources for quantum information applications like quantum key distribution.

To further improve the emission efficiency of singlephoton sources, the application of optical cavities is an essential topic. As shown in Figure 12f, Iff et al. proposed a deterministic single-photon source based on the integration of WSe<sub>2</sub> QDs with a circular Bragg grating cavity [236]. The cavity enhances SE through the Purcell effect, thereby improving the efficiency and scalability of the single-photon source. The use of the circular Bragg grating cavity enables deterministic placement of QDs and strain-induced formation, significantly enhancing emission. This provides a new approach for developing a single-photon emitter that is simple to manufacture, cost-effective, and performs well.

Despite the remarkable performance of 2D semiconductor single-photon sources in terms of efficient SPE and tunability, challenges remain in integrating these devices into practical quantum information processing systems. Currently, individual or small numbers of 2D single-photon sources have been validated in laboratory settings [19], [225], [226], [232], [233], [236], but these isolated devices struggle to meet the demands for high integration and stability in real-world applications. To solve this problem, the measures of combining 2D semiconductor single-photon sources with mature chip manufacturing technologies are beginning to be explored. Through on-chip integration, device miniaturization and mass production can be realized, enhancing system reliability and scalability. This advancement paves the way for the practical application of quantum information technologies and represents a key direction for future research.

Blauth et al. integrated WSe<sub>2</sub> monolayer quantum emitters with metal plasmonic waveguides for nanoscale singlephoton generation and routing (Figure 13a) [237]. The emitter was positioned close to the waveguide edge (Figure 13b), enabling on-chip single-photon sources suitable for quantum information and optical communication. Strain engineering and hBN encapsulation could enhance coupling efficiency and emitter quality [238]-[241]. And in 2019, Peyskens et al. used a dry-transfer method to integrate WSe<sub>2</sub> flakes onto SiN waveguides, achieving efficient light confinement for on-chip transmission (Figure 13c) [242]. Confocal PL scans (Figure 13d) and PL collected via fiber (Figure 13e) confirmed enhanced emission on the waveguide, highlighting its scalability for quantum photonic chips without complex postprocessing.

As previously mentioned, when discussing roomtemperature single-photon sources, it is imperative to consider hBN, as it is capable of producing narrowband SPE across a wide temperature range, including room temperature [17], [243] – [247], thereby making it an ideal material for quantum emitters. hBN emitters integrated with AlN waveguides demonstrated room-temperature SPE and coupling (Figure 13f and g) [248]. Photons successfully coupled into

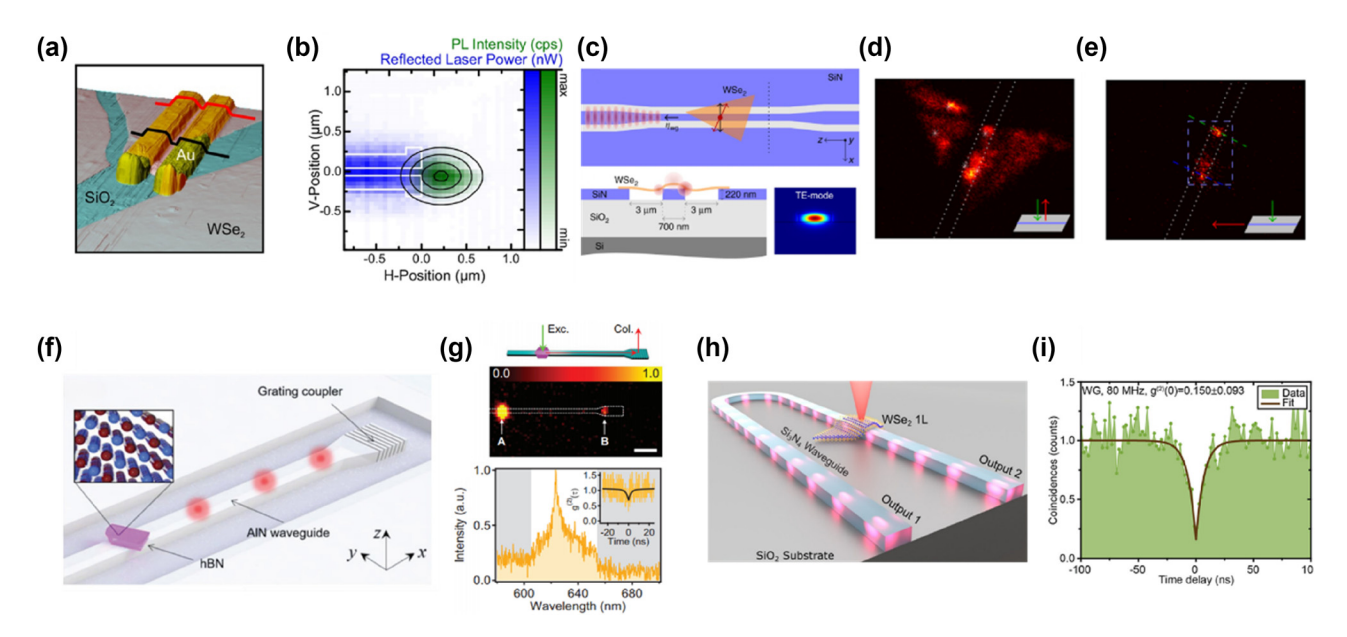


**Figure 13:** On-chip integration of 2D SPE emitters. (a) False-color perspective view of an atomic force microscope image of the combined plasmonic waveguide and monolayer WSe<sub>2</sub> system. (b) The relative position of the QD and waveguide as obtained from high-resolution PL and laser reflectivity scans. Panel (a–b): reproduced from ref. [237]. Copyright 2018, American Chemical Society. (c) Upper panel: schematic of the device integrating a WSe<sub>2</sub> flake onto a SiN waveguide. Lower panel: a cross-sectional view of the sample (left) and a cross-sectional mode profile (at 750 nm) of the waveguide (right). (d) PL scan from the top of the sample. (e) Waveguide-coupled PL scan collected through the fiber. Panel (c–e): reproduced from ref. [242]. Copyright 2019, Springer Nature. (f) Schematic of the hybrid system, where an hBN flake is integrated onto an AlN waveguide. (g) Top panel: schematic of the nonlocal collection scheme. Emission from the grating coupler of the waveguide (spot B) could be collected. Bottom panel: PL spectrum collected from spot B (the grating coupler). The inset in the figure shows the second-order autocorrelation function  $g^{(2)}(\tau)$ , panel (f–g): reproduced from ref. [248]. Copyright 2019, Wiley-VCH. (h) Schematic of the coupled WSe<sub>2</sub> monolayer on the Si<sub>3</sub>N<sub>4</sub> waveguide. (i) The result of the second-order autocorrelation measurement conducted through waveguide output 1 ( $g^{(2)}(0) = 0.150 \pm 0.093$ ). Panel (h–i): reproduced from ref. [249]. Copyright 2021, American Chemical Society.

the waveguide and were transmitted through the grating coupler confirming SPE.

In 2021, Herranz et al. utilized SiN waveguide edges to create strain-induced single-photon emitters in WSe<sub>2</sub>, achieving effective waveguide coupling (Figure 13h) [249]. Emission analysis showed  $g^{(2)}(0) = 0.150$ , confirming SPE through waveguide coupling (Figure 13i). These results confirm the single-photon nature of the emission, indicating that, despite background noise, the quality of SPE is maintained through waveguide coupling.

## 5 Other types of 2D photonic source

In the preceding sections, we have comprehensively reviewed lasers and single-photon sources based on 2D vdW materials, highlighting their exceptional performance in optics and quantum optics, such as high gain, tunability, and stability at room temperature. These attributes establish 2D vdW materials as strong candidates for next-generation optoelectronic devices. However, the optical properties of 2D vdW materials extend beyond the domain of linear

optics; they also exhibit significant potential in nonlinear optics. Notably, phenomena such as HHG and P-band emission have demonstrated unique advantages in 2D vdW materials.

The HHG response in 2D vdW materials makes it suitable for integrated nonlinear nanophotonic devices, such as optical modulators [250] and optical switches [251]. HHG can produce significant nonlinear optical responses under low-intensity laser conditions [252], which helps in the realization of more efficient and compact optical devices. In recent years, HHG in 2D vdW materials has attracted significant research interest [253]–[255]. However, enhancing HHG intensity and achieving more effective control over the process remain key challenges that warrant further exploration.

Säynätjoki et al. investigated the nonlinear optical responses of monolayer MoS<sub>2</sub>, focusing on third-harmonic generation (THG) and fourth-harmonic generation [256]. The second-harmonic generation (SHG) map (Figure 14a, top panel) shows SHG in monolayer MoS<sub>2</sub> but not in bilayer MoS<sub>2</sub>, as SHG requires noncentrosymmetry, which is absent in bilayers [25], [257]. One of the notable discoveries in this

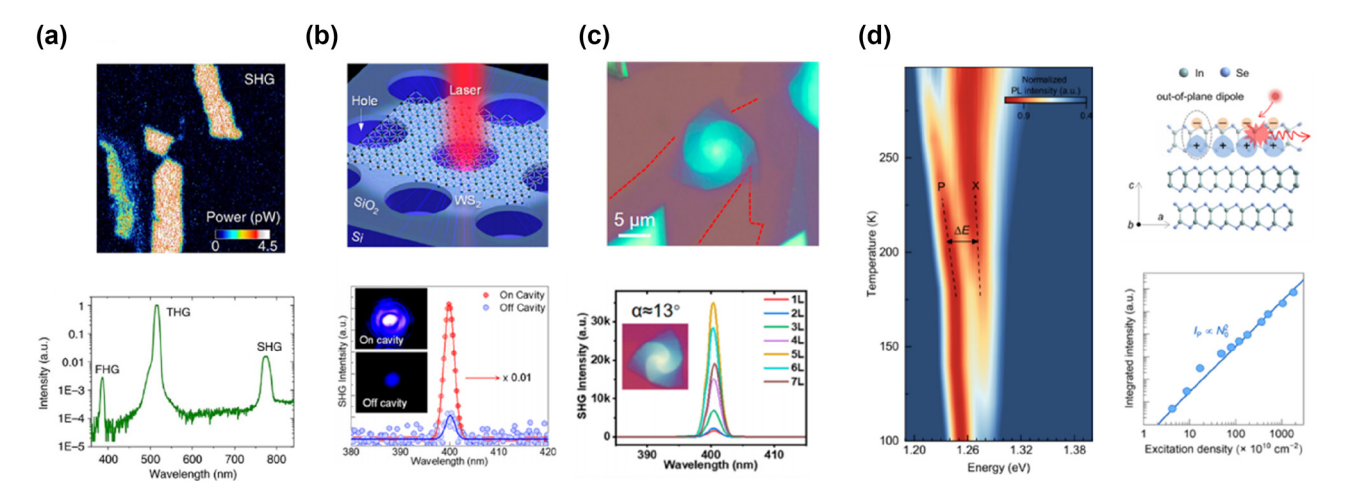


Figure 14: Tuning of high-order harmonic generation and exciton - exciton scattering induced P-band emission. (a) Top panel: the SHG map of MoS<sub>2</sub> flakes. Bottom panel: the PL spectrum of the nonlinear signal from the monolayer MoS<sub>2</sub>, Reproduced from ref. [256]. Copyright 2017, Springer Nature. (b) Top panel: schematic of the WS<sub>2</sub> monolayer placed on a silicon substrate with holes. Bottom panel: the SHG spectra collected from the WS<sub>2</sub> monolayer on cavity (red) and off cavity (blue) under excitation with an 800 nm fs pulsed laser. Insets: the microscope image of SHG emission from the WS<sub>2</sub> monolayer in the on-cavity and off-cavity regions. Reproduced from ref. [266]. Copyright 2022, American Chemical Society. (c) Top panel: the optical microscopy images of a right-handed supertwisted WS<sub>2</sub> spiral with a twist angle of approximately 17°. Bottom panel: the SHG spectra of supertwisted WS<sub>2</sub> spirals with a twist angle of around 13°, demonstrating the SHG response for different layer numbers. The SHG intensity gradually increases from 1 to 5 layers and then drops rapidly from 6 to 7 layers, indicating different nonlinear optical properties in the twisted structure depending on the layer number. Reproduced from ref. [267]. Copyright 2024, American Chemical Society. (d) Left panel: the PL spectra of an exfoliated InSe crystal under different temperatures, ranging from 298 K to 100 K. Right panel (upper): the side view of the γ-phase InSe crystal structure, highlighting the out-of-plane dipole moment and the inhomogeneous charge distribution of excitons. Right panel (lower): the relationship between the P-band emission intensity and the excitation density. Reproduced from ref. [27]. Copyright 2023, American Chemical Society.

study is the observation that THG is significantly stronger than SHG (Figure 14a, bottom panel), contrary to conventional expectations where the efficiency of higher-order harmonic processes is typically weaker [258], [259]. The key reason behind this unexpected result lies in the trigonal warping of the electronic band structure of MoS<sub>2</sub>. The lack of spatial inversion symmetry plays a critical role – though it alone is insufficient for generating SHG, the combination of noncentrosymmetric band structure and trigonal warping facilitates efficient harmonic generation [93], [260]-[265].

In terms of integration with microcavities, Shi et al. enhanced SHG in WS2 by placing a monolayer over a patterned silicon substrate to create a Fabry-Pérot microcavity, amplifying SHG by up to 1,580 times (Figure 14b) [266]. Coupling WS<sub>2</sub> with cavity modes at the excitation wavelength (820 nm) resulted in electric field amplification and improved directionality (with a divergence angle of  $\sim$ 5°), crucial for applications in integrated photonics and optoelectronics.

Recently, Tong et al. demonstrated the synthesis of supertwisted WS<sub>2</sub> spirals and their effect on nonlinear optical properties [267]. Using a water-assisted CVD method, the spirals were grown on non-Euclidean surfaces to achieve different twist angles (Figure 14c, top panel). The study observed an oscillatory dependence of SHG intensity on the layer number of the supertwisted spirals, which is attributed to phase matching of nonlinear dipoles within different layers (Figure 14c, bottom panel). Additionally, varying the twist angle resulted in different periodic structures that enabled inversion symmetry breaking, leading to an enhancement in the SHG signal by a factor of 2-136 compared with a single-layer structure.

As an important aspect of nonlinear optics in 2D vdW materials, p-band emission has received much research attention in recent years, especially concerning its related properties at room temperature. P-band emission is a superlinear and low-coherence light emission phenomenon driven by exciton–exciton scattering [268], [269], providing a low-coherence, high-intensity light source at low power, holding promise for applications in speckle-free imaging [270], [271], frequency-resolved lidar [272], and interferometric sensing [273], [274].

Liang et al. investigated exciton dynamics and P-band emissions in exfoliated InSe, revealing P-band emission under CW excitation at low excitation density ( $\sim 10^{10}$  cm<sup>-2</sup>), unlike typical superlinear emissions requiring high densities and pulsed modes [275]-[279]. This is enabled by strong exciton-exciton scattering, due to enhanced spatial confinement and unique material properties of InSe. The γ-phase InSe structure with an out-of-plane dipole orientation supports efficient exciton scattering (right panel of Figure 14d, upper) [29], [143], [144], [147]. P-band intensity followed a quadratic dependence on exciton density (right panel of Figure 14d, lower), confirming pair scattering as the emission source. Cooling caused a blue shift in P-band and X-peak energies, indicating increased exciton stability and reduced phonon scattering. Meanwhile, energy difference between P-band and X-peak energies increases from 29.1 meV to 49.8 meV (Figure 14d, left panel), which is attributed to increased kinetic energy loss during scattering as the temperature rises. Higher temperatures result in increased kinetic energy for the excitons, which means that more energy is converted to other forms, such as heat or phonon energy, during exciton-exciton scattering, leading to an increased energy difference, which supports the exciton-exciton scattering model [269], [280]. This work demonstrates strong excitonic interactions in InSe, paying the way for efficient low-coherence light sources and near-infrared optoelectronic devices.

# 6 Electrically driven 2D photonic sources

The implementation of electrical pumping operation is a significant milestone toward the practical application of emergent 2D vdW light sources [281]. During the device structure design, the key step is to enable effective injections of charge carriers into 2D vdW semiconductors to promote light emission, as has always been one of the core issues concerned in the traditional semiconductor field [282]-[284]. So far, the widely used carrier injection techniques mainly include electrostatic doping, tunneling junction, band alignment engineering, and alternating current driven injection [285]. In the early stages of research, several groups developed various types of LEDs based on 2D vdW semiconductors, and the external quantum efficiency (EQE) of such exciton emission dominated devices at room temperature reached up to 5 % [197], [286]-[291].

A significant issue is that the external quantum efficiency (EQE) of early 2D LEDs (up to  $\sim$ 5 %) is significantly lower than the PL quantum yield (approximately 20 %) of the intrinsic 2D materials. The potential causes may include the exacerbation of nonradiative recombination channels, such as scattering caused by defects at the device interfaces, exciton-exciton annihilation at high carrier concentrations, nonradiative recombination involving exciton complexes at high doping levels, ineffective or unbalanced carrier injection, carrier leakage, and low optical outcoupling efficiency [290], [292]-[295]. While addressing these issues simultaneously to further enhance the EQE remains challenging, some research groups have made attempts. For example, in 2020, Kwon et al. demonstrated a WSe2-based light-emitting transistor, which included a monolayer WSe2 channel and graphene contacts, coupled with two separate top metal gates [296]. By adjusting the contact barrier height, the type and density of injected charge carriers could be independently controlled to achieve balanced injection, resulting in bright emission near 750 nm with a high peak EOE of  $\sim$ 6 % at room temperature. Similarly, in 2024, Shin et al. also utilized a double-gate structure (containing graphene and silicon gates) to develop a WSe<sub>2</sub>-based light-emitting transistor with balanced electron and hole injection [297]. Furthermore, with the help of a local graphene gate, electrons and holes could flow into the 1D region to form neutral excitons. The in-plane electric field within the 1D region effectively confines the neutral excitons and expels charged excitons through charge interaction, thus enhancing the efficiency of radiative recombination dominated by neutral excitons. The demonstrated device exhibits an improved maximum EQE of ~8.2 % at room temperature. To achieve high-performance midinfrared LEDs, Gupta et al. placed the light-emitting BP/MoS<sub>2</sub> heterostructure on Al<sub>2</sub>O<sub>3</sub>/Au to form a vertical resonant cavity, which simultaneously enhances the SE rate via Purcell effect and light outcoupling efficiency by appropriately designing the cavity length [298]. In addition, a transparent indium tin oxide conductive layer at the top can reduce the parasitic resistance while having almost no impact on light output. The measured operating wavelength is 3.65 µm with an EQE of 4.43 %, and the overall performance exceeds that of commercial mid-infrared LEDs, comparable to the interband cascade lasers.

Compared to weakly coupled devices, EP LEDs in the strong coupling regime offer higher regulatory flexibility. Gu et al. reported the first room-temperature EP LED based on 2D vdW materials, where multiple WS<sub>2</sub> monolayers serve as the active layers to enhance exciton density, hBN serves as the tunneling spacer layer, and graphene serves as the transparent conductive layer (Figure 15a [299]). The above structure is embedded in the bottom DBR (consisting of 12 pairs of SiO<sub>2</sub>/SiN, with a metal electrode deposited on the surface) and the top silver/PMMA film to detect the EP emission. Angle-resolved electroluminescence spectra indicate the emission follows the dispersion feature of EPs, with the emission angle confined within  $\pm 15^{\circ}$  (Figure 15b). The device displays an EQE of 0.1 %, comparable to the performance of organic molecule- and carbon nanotube-based EP LEDs reported at the time.

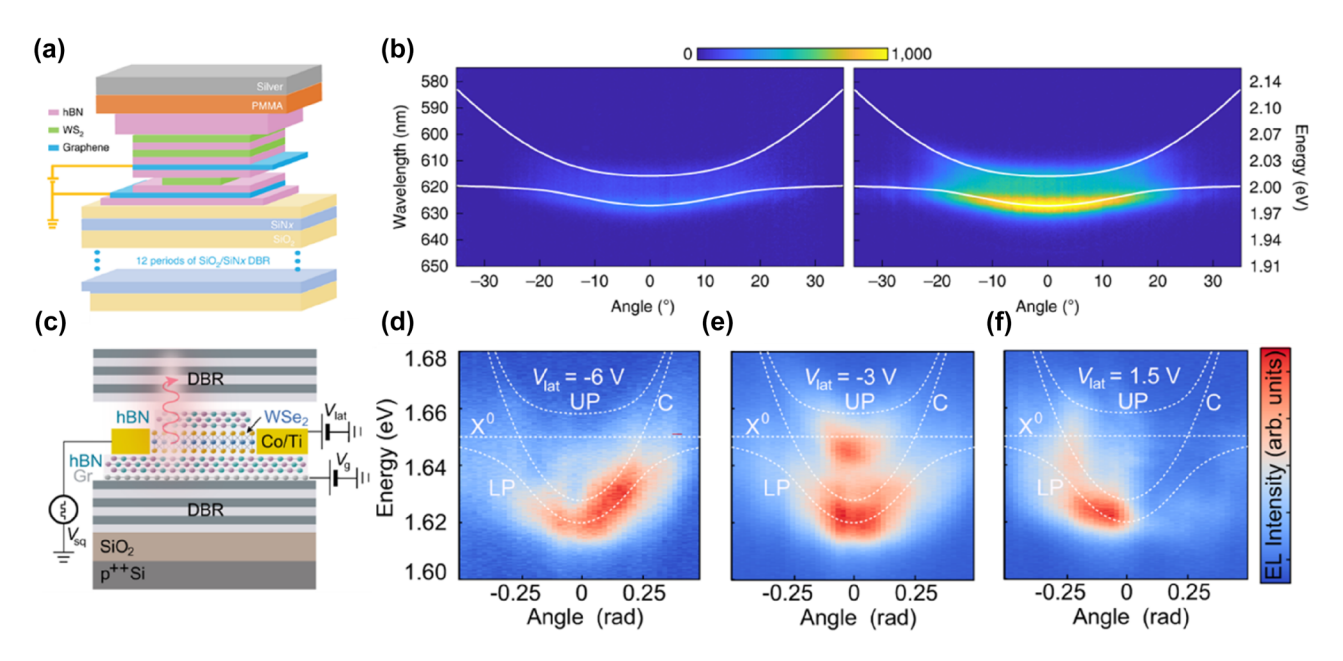


Figure 15: Electrically pumped EP LEDs. (a) Schematic of an electrically pumped EP LED with different layers of the vdW heterostructure embedded inside a bottom DBR and top silver mirrors. (b) Angle-resolved PL (left panel) and electroluminescence (right panel) of the device in (a). Reproduced from ref. [299]. Copyright 2019, Springer Nature. (c) Schematic of an electrically pumped EP LED with electrical control of polarization and emission angle. (d-f) Angle-resolved electroluminescence spectra at the lateral voltage of -6 V (d), -3 V (e), and 1.5 V (f) of the device in (c). Reproduced from ref. [301]. Copyright 2022, Springer Nature.

Since EPs possess both excitonic and photonic characteristics, real-time tuning of the emission properties can be achieved by electrically controlling the carrier properties [300]. Marin et al. further demonstrated an EP LED with room-temperature electrical control of emission polarization (polarization ratio ranging from 20 % to -20 %) and emission angle (from negative to positive [301]). The working principle involves applying a voltage to the electrode deposited above the WSe<sub>2</sub> monolayer, which alters the band alignment and the overall external electric field, thereby modulating the in-plane carrier velocity and spatial distribution (Figure 15c). Through strong exciton-photon coupling, the change in the in-plane exciton momentum is inherited by the EP and converted into different photon emission angles (Figure 15d-f). Simultaneously, the change in the exciton momentum also alters the exciton energy at the K and K' points, leading to a change in the valley EP population and strong valley polarization.

Furthermore, achieving electrically pumped singlephoton sources is critical for the development of practical on-chip quantum emitters [302]. An early example was reported by Berraquero et al. where the device is based on a single tunneling junction including Au/WSe<sub>2</sub>/hBN/ graphene/Au on a SiO<sub>2</sub>/Si substrate (Figure 16a [303]). Electroluminescence spectra at 10 K reveal several narrow emission peaks with linewidths ranging from 0.8 to 3 nm in the 750-850 nm range. The intensity-correlation function exhibits the antibunched nature with a  $g^{(2)}(0)$  of 0.29  $\pm$ 0.08, expected for a single-photon source. Using WS2 with a larger bandgap, the SPE wavelength can be extended from the near-infrared to the visible range ( $\sim$ 640 nm). At the same time, other research groups also observed similar electrically pumped single defect emission using tunneling junctions [304], [305].

For untreated materials, defects are usually randomly distributed, so another key issue is to customize the position of the single-photon emitter. Advanced strategies include using atomic force microscopy or scanning tunneling microscopy tips to generate on-demand atomic-level defects to localize excitons [306], [307]. Recently, Guo et al. introduced an array of Au nanopillars embedded in the WSe2 based device to simultaneously inject carriers and generate ordered strain (Figure 16b), ultimately producing a site-controlled electrically injected SPE with a  $g^{(2)}(0)$  of  $0.32 \pm 0.01$  [308].

It is worth noting that electrically driven SPE has only been realized in TMD materials, which primarily results from excitons bound to defects with small binding energies and only operates at cryogenic temperatures. Besides, the observed SPE is generally accompanied by strong emission backgrounds associated with other excitonic processes, leading to a relatively low single-photon purity. The hBN has acted as a potential candidate for room-temperature

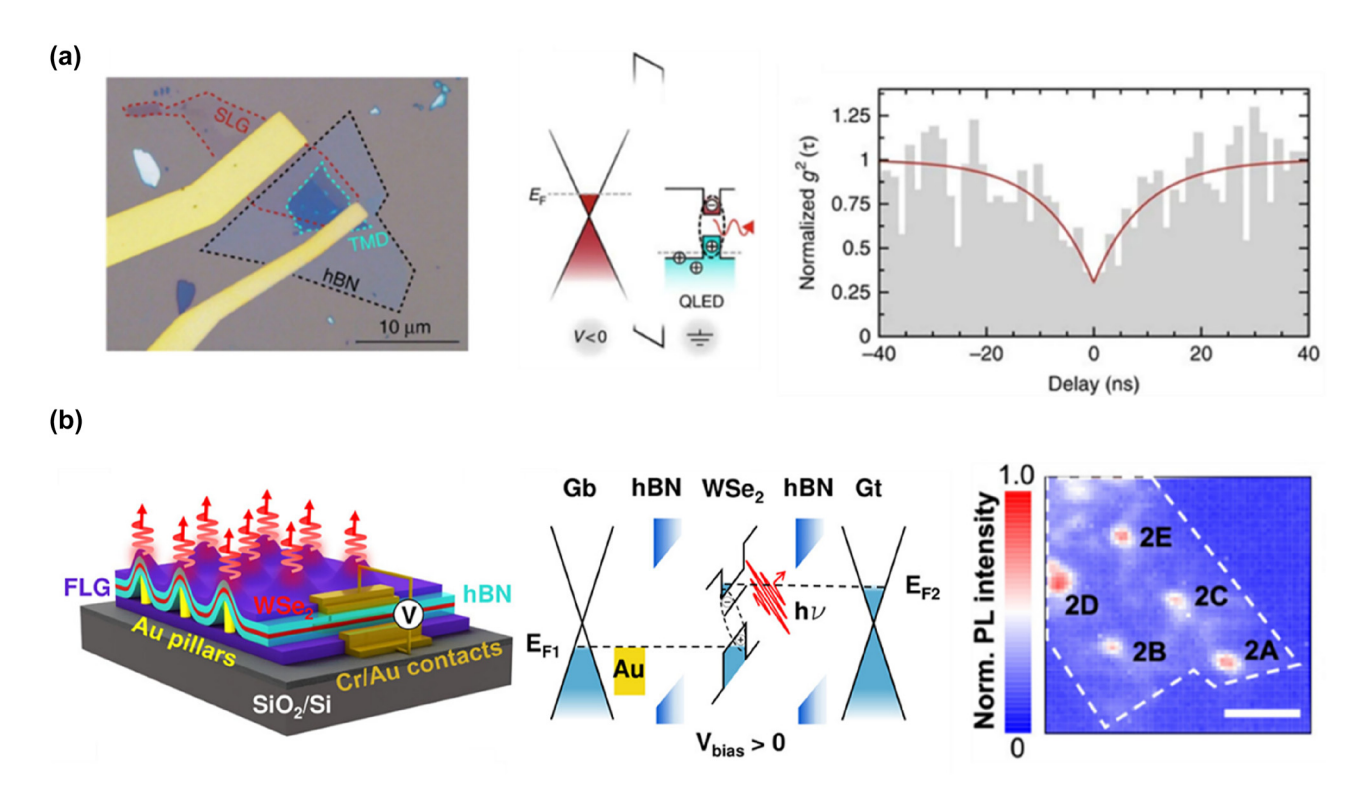


**Figure 16:** Electrically pumped single-photon sources. (a) Left panel: optical image of an electrically pumped single-photon source including Au/WSe<sub>2</sub>/hBN/graphene/Au on the SiO<sub>2</sub>/Si substrate. Middle panel: energy band diagram with applied bias. Right panel: intensity-correlation function of the electroluminescence signal. Reproduced from ref. [303]. Copyright 2016, Springer Nature. (b) Left panel: schematic of an electrically pumped single-photon source, including graphene/hBN/WSe<sub>2</sub>/hBN/Au pillars/graphene. Middle panel: energy band diagram with applied bias. Right panel: electroluminescence mapping over the active region. Reproduced from ref. [308]. Copyright 2023, American Chemical Society.

high-purity SPE, but achieving effective electrical injection remains an unresolved challenge [229], [309].

### 7 Conclusion and outlook

In this review, we provide an in-depth introduction of lightemission properties and advancements in 2D vdW materials, specifically focusing on various light sources, such as lasers, single-photon sources, and nonlinear optical applications. The review highlights several aspects of 2D vdW materials, including their unique excitonic properties, the principles of light emission, and the development of semiconductor lasers based on these materials. It covers advancements in intralayer and interlayer exciton lasers, cavity-free laser systems, and EP emissions, emphasizing the integration potential of SPE sources in on-chip systems and exploring the nonlinear optical properties, like HHG and P-band emission. Lastly, we introduce electrically pumped light sources.

Moving forward, in the field of lasers, optimizing the laser structure of 2D vdW materials offers the potential to

significantly lower the lasing threshold, enabling the development of low-power, continuous-wave laser sources. These sources are particularly suited for portable devices and energy-critical applications, such as biosensors and on-chip communication. The EP interactions inherent in 2D vdW materials are ideally suited for on-chip photonic integration, which can greatly enhance the efficiency and miniaturization of photonic systems, with wide-ranging applications in optical communication and quantum information processing. In the realm of single-photon sources, 2D vdW materials hold great promise for high-purity single-photon generation, supporting advances in quantum communication and quantum computing. As material stacking technologies continue to progress, the role of 2D vdW materials in the field of quantum information will expand further. Additionally, the nonlinear optical properties of 2D vdW materials provide new opportunities for creating compact, tunable photonic devices. Furthermore, the unique electronic and optical characteristics of 2D vdW materials allow for integration into multifunctional, complex devices, enabling the combination of various functions such as light emission, detection, and modulation. This integration could

significantly reduce system costs while enhancing device performance. At the same time, 2D vdW materials exhibit excellent stability at room temperature, allowing them to operate across a wider range of temperatures, making them ideal for diverse applications, from space missions to industrial environments, without the need for additional cooling.

However, realizing these prospects presents several technical challenges. Current fabrication techniques for 2D vdW materials, such as mechanical exfoliation, are limited in terms of scalability and cannot meet commercial production demands. To enable the widespread use of 2D vdW materials, reliable large-scale production methods, such as CVD, must be developed. These methods need to ensure the production of high-quality, defect-free materials, while also allowing for precise control over layer thickness and composition. Additionally, the sensitivity of 2D vdW materials to external factors such as electric and magnetic fields make it difficult to achieve precise and stable control over their properties. Maintaining the stability of these properties in varying environmental conditions is a key challenge for improving the reliability of devices. 2D vdW materials are often integrated with other materials or substrates, but the interface interactions between them can degrade performance, leading to a loss of optical and electronic properties. Therefore, optimizing these interfacial interactions and employing techniques such as surface passivation or encapsulation are essential for enhancing device performance. Despite the significant potential of 2D vdW materials for SPE, maintaining their stability and photon purity - especially in complex environments - remains a challenge. Controlling noise and ensuring photon purity are critical for improving their reliability in quantum information applications. Finally, many 2D vdW materials exhibit an indirect bandgap in their multilayer or bulk forms, which limit their light emission efficiency. Research focused on achieving efficient lasing or SPE in multilayer structures, or on maintaining direct bandgap characteristics in thicker layers, will be key to advancing the application of 2D vdW materials in integrated photonics.

In summary, while the potential of 2D vdW materials in photonics is immense, overcoming the current challenges in fabrication, material integration, and performance stability will be crucial for realizing their full potential in nextgeneration optical and quantum devices.

**Research funding:** LZ acknowledges funding support from the National Natural Science Foundation of China (No. 62304117) and the Natural Science Foundation of Shandong Province (No. ZR2023QF049). QZ acknowledges funding support from the National Natural Science Foundation of China (Nos. U23A2076, 51991340, 52072006) and the Beijing National Natural Science Foundation (No. JQ21004).

Author contributions: This review was leaded by QZ and LZ. KT and CL drafted the manuscript. All authors have accepted responsibility for the entire content of this manuscript and approved its submission.

**Conflict of interest:** Authors state no conflicts of interest. Informed consent: Informed consent was obtained from all individuals included in this study.

**Ethical approval:** The conducted research is not related to either human or animals use.

**Data availability:** Data sharing is not applicable to this article as no datasets were generated or analyzed during the current study.

#### References

- [1] K. F. Mak, C. Lee, J. Hone, J. Shan, and T. F. Heinz, "Atomically thin MoS<sub>2</sub>: a new direct-gap semiconductor," Phys. Rev. Lett., vol. 105, no. 13, p. 136805, 2010.
- [2] A. Chernikov, et al., "Exciton binding energy and nonhydrogenic rydberg series in monolayer WS<sub>2</sub>," Phys. Rev. Lett., vol. 113, no. 7, p. 076802, 2014.
- [3] A. Splendiani, et al., "Emerging photoluminescence in monolayer MoS<sub>2</sub>," *Nano Lett.*, vol. 10, no. 4, pp. 1271–1275, 2010.
- [4] X. Liu, et al., "Strong light—matter coupling in two-dimensional atomic crystals," Nat. Photonics, vol. 9, no. 1, pp. 30-34, 2015.
- [5] K. S. Kim, et al., "Large-scale pattern growth of graphene films for stretchable transparent electrodes," Nature, vol. 457, no. 7230, pp. 706-710, 2009.
- [6] A. K. Geim and I. V. Grigorieva, "Van der Waals heterostructures," Nature, vol. 499, no. 7459, pp. 419-425, 2013.
- [7] X. Li, et al., "Large-area synthesis of high-quality and uniform graphene films on copper foils," Science, vol. 324, no. 5932, pp. 1312-1314, 2009.
- [8] K. S. Novoselov, et al., "Electric field effect in atomically thin carbon films," Science, vol. 306, no. 5696, pp. 666-669, 2004.
- [9] M. Xu, T. Liang, M. Shi, and H. Chen, "Graphene-like two-dimensional materials," Chem. Rev., vol. 113, no. 5, pp. 3766 - 3798, 2013.
- [10] G. Wang, et al., "Colloquium: excitons in atomically thin transition metal dichalcogenides," Rev. Mod. Phys., vol. 90, no. 2, p. 021001, 2018.
- [11] R. Sundaram, et al., "Electroluminescence in single layer MoS<sub>2</sub>," Nano Lett., vol. 13, no. 4, pp. 1416-1421, 2013.
- [12] S. Wu, et al., "Monolayer semiconductor nanocavity lasers with ultralow thresholds," *Nature*, vol. 520, no. 7545, pp. 69-72, 2015.
- [13] B. Radisavljevic, A. Radenovic, J. Brivio, V. Giacometti, and A. Kis, "Single-layer MoS<sub>2</sub> transistors," Nat. Nanotechnol., vol. 6, no. 3, pp. 147-150, 2011.
- [14] M. Bernardi, M. Palummo, and J. C. Grossman, "Extraordinary sunlight absorption and one nanometer thick photovoltaics using two-dimensional monolayer materials," Nano Lett., vol. 13, no. 8, pp. 3664-3670, 2013.

- [15] M. Chhowalla, H. S. Shin, G. Eda, L. J. Li, K. P. Loh, and H. Zhang, "The chemistry of two-dimensional layered transition metal dichalcogenide nanosheets," Nat. Chem., vol. 5, no. 4, pp. 263 - 275, 2013.
- [16] Q. H. Wang, K. Kalantar-Zadeh, A. Kis, J. N. Coleman, and M. S. Strano, "Electronics and optoelectronics of two-dimensional transition metal dichalcogenides," Nat. Nanotechnol., vol. 7, no. 11, pp. 699-712, 2012.
- [17] T. T. Tran, K. Bray, M. J. Ford, M. Toth, and I. Aharonovich, "Quantum emission from hexagonal boron nitride monolayers," Nat. Nanotechnol., vol. 11, no. 1, pp. 37-41, 2016.
- [18] A. Srivastava, M. Sidler, A. V. Allain, D. S. Lembke, A. Kis, and A. Imamoğlu, "Optically active quantum dots in monolayer WSe<sub>2</sub>," *Nat. Nanotechnol.*, vol. 10, no. 6, pp. 491–496, 2015.
- [19] Y. M. He, et al., "Single quantum emitters in monolayer semiconductors," Nat. Nanotechnol., vol. 10, no. 6, pp. 497-502,
- [20] I. Aharonovich, D. Englund, and M. Toth, "Solid-state single-photon emitters," Nat. Photonics, vol. 10, no. 10, pp. 631-641, 2016.
- [21] A. Gottscholl, et al., "Spin defects in hBN as promising temperature, pressure and magnetic field quantum sensors," Nat. Commun., vol. 12, no. 1, p. 4480, 2021.
- [22] L. M. Malard, T. V. Alencar, A. P. M. Barboza, K. F. Mak, and A. M. de Paula, "Observation of intense second harmonic generation from MoS<sub>2</sub> atomic crystals," Phys. Rev. B Condens. Matter Mater. Phys., vol. 87, no. 20, p. 201401, 2013.
- [23] C. Janisch, et al., "Extraordinary second harmonic generation in tungsten disulfide monolayers," Sci. Rep., vol. 4, no. 1, p. 5530,
- [24] Y. Li, et al., "Measurement of the optical dielectric function of monolayer transition-metal dichalcogenides: MoS<sub>2</sub>, MoSe<sub>2</sub>, WS<sub>2</sub>, and WSe<sub>2</sub>," Phys. Rev. B, vol. 90, no. 20, p. 205422,
- [25] N. Kumar, et al., "Second harmonic microscopy of monolayer MoS<sub>2</sub>," Phys. Rev. B Condens. Matter Mater. Phys., vol. 87, no. 16, p. 161403, 2013.
- [26] J. Hong, et al., "Exploring atomic defects in molybdenum disulphide monolayers," Nat. Commun., vol. 6, no. 1, p. 6293,
- [27] Y. Liang, et al., "Strong exciton exciton scattering of exfoliated van der Waals InSe toward efficient continuous-wave near-infrared P-band emission," Nano Lett., vol. 23, no. 9, pp. 4058-4065, 2023.
- [28] X. Liu, et al., "Whispering gallery mode lasing from hexagonal shaped layered lead iodide crystals," ACS Nano, vol. 9, no. 1, pp. 687-695, 2015.
- [29] C. Li, et al., "Room-temperature near-infrared excitonic lasing from mechanically exfoliated InSe microflake," ACS Nano, vol. 16, no. 1, pp. 1477-1485, 2021.
- [30] S. Kang, et al., "Coherent many-body exciton in van der Waals antiferromagnet NiPS<sub>3</sub>," Nature, vol. 583, no. 7818, pp. 785-789,
- [31] C. Li, et al., "2D CrSBr enables magnetically controllable exciton-polaritons in an open cavity," Adv. Funct. Mater., p. 2411589, 2024, https://doi.org/10.1002/adfm.202411589.
- [32] E. Jung, J. C. Park, Y. S. Seo, J. H. Kim, J. Hwang, and Y. H. Lee, "Unusually large exciton binding energy in multilayered 2H-MoTe<sub>2</sub>," Sci. Rep., vol. 12, no. 1, p. 4543, 2022.

- [33] G. Zhang, et al., "Determination of layer-dependent exciton binding energies in few-layer black phosphorus," Sci. Adv., vol. 4, no. 3, p. eaap9977, 2018.
- [34] N. Saigal, V. Sugunakar, and S. Ghosh, "Exciton binding energy in bulk MoS<sub>2</sub>: a reassessment," Appl. Phys. Lett., vol. 108, no. 13, 2016. https://doi.org/10.1063/1.4945047.
- [35] A. Beal and W. Liang, "Excitons in 2H-WSe<sub>2</sub> and 3R-WS<sub>2</sub>," J. Phys. C: Solid State Phys., vol. 9, no. 12, p. 2459, 1976.
- [36] A. Arora, M. Koperski, K. Nogajewski, J. Marcus, C. Faugeras, and M. Potemski, "Excitonic resonances in thin films of WSe<sub>2</sub>: from monolayer to bulk material," Nanoscale, vol. 7, no. 23, pp. 10421-10429, 2015.
- [37] A. Klots, et al., "Probing excitonic states in suspended two-dimensional semiconductors by photocurrent spectroscopy," Sci. Rep., vol. 4, no. 1, p. 6608, 2014.
- [38] M. M. Ugeda, et al., "Giant bandgap renormalization and excitonic effects in a monolayer transition metal dichalcogenide semiconductor," Nat. Mater., vol. 13, no. 12, pp. 1091–1095, 2014.
- [39] J. Yang, et al., "Robust excitons and trions in monolayer MoTe<sub>2</sub>," ACS Nano, vol. 9, no. 6, pp. 6603-6609, 2015.
- [40] B. Zhu, H. Zeng, J. Dai, Z. Gong, and X. Cui, "Anomalously robust valley polarization and valley coherence in bilayer WS<sub>2</sub>," *Proc. Natl. Acad. Sci. U. S. A.*, vol. 111, no. 32, pp. 11606—11611, 2014.
- [41] K. He, et al., "Tightly bound excitons in monolayer WSe<sub>2</sub>," Phys. Rev. Lett., vol. 113, no. 2, p. 026803, 2014.
- [42] M. Kang, et al., "Universal mechanism of band-gap engineering in transition-metal dichalcogenides," Nano Lett., vol. 17, no. 3, pp. 1610 - 1615, 2017.
- [43] S. Smolenski, et al., "Large exciton binding energy in the Bulk van der Waals magnet CrSBr," arXiv preprint arXiv:2403.13897,
- [44] K. F. Mak, K. He, J. Shan, and T. F. Heinz, "Control of valley polarization in monolayer MoS<sub>2</sub> by optical helicity," Nat. Nanotechnol., vol. 7, no. 8, pp. 494-498, 2012.
- [45] H. Zeng, J. Dai, W. Yao, D. Xiao, and X. Cui, "Valley polarization in MoS<sub>2</sub> monolayers by optical pumping," Nat. Nanotechnol., vol. 7, no. 8, pp. 490-493, 2012.
- [46] X. Xu, W. Yao, D. Xiao, and T. F. Heinz, "Spin and pseudospins in layered transition metal dichalcogenides," Nat. Phys., vol. 10, no. 5, pp. 343-350, 2014.
- [47] J. F. Sierra, J. Fabian, R. K. Kawakami, S. Roche, and S. O. Valenzuela, "Van der Waals heterostructures for spintronics and opto-spintronics," Nat. Nanotechnol., vol. 16, no. 8, pp. 856–868, 2021.
- [48] J. T. Gish, D. Lebedev, T. W. Song, V. K. Sangwan, and M. C. Hersam, "Van der Waals opto-spintronics," Nat. Electron., pp. 1-12, 2024, https://doi.org/10.1038/s41928-024-01167-3.
- [49] H. Shi, et al., "Exciton dynamics in suspended monolayer and few-layer MoS<sub>2</sub> 2D crystals," ACS Nano, vol. 7, no. 2, pp. 1072 - 1080, 2013.
- [50] C. Jin, E. Y. Ma, O. Karni, E. C. Regan, F. Wang, and T. F. Heinz, "Ultrafast dynamics in van der Waals heterostructures," Nat. Nanotechnol., vol. 13, no. 11, pp. 994-1003, 2018.
- [51] P. Rivera, et al., "Observation of long-lived interlayer excitons in monolayer MoSe<sub>2</sub> – WSe<sub>2</sub> heterostructures," Nat. Commun., vol. 6, no. 1, p. 6242, 2015.
- [52] P. Rivera, et al., "Valley-polarized exciton dynamics in a 2D semiconductor heterostructure," Science, vol. 351, no. 6274, pp. 688 - 691, 2016.

- [53] B. Miller, et al., "Long-lived direct and indirect interlayer excitons in van der Waals heterostructures," Nano Lett., vol. 17, no. 9, pp. 5229-5237, 2017.
- [54] J. Kim, et al., "Observation of ultralong valley lifetime in WSe<sub>2</sub>/MoS<sub>2</sub> heterostructures," Sci. Adv., vol. 3, no. 7, p. e1700518,
- [55] C. Jiang, et al., "Microsecond dark-exciton valley polarization memory in two-dimensional heterostructures," Nat. Commun., vol. 9, no. 1, p. 753, 2018.
- [56] A. Arora, et al., "Highly anisotropic in-plane excitons in atomically thin and bulklike 1 T'-ReSe<sub>2</sub>," Nano Lett., vol. 17, no. 5, pp. 3202-3207, 2017.
- [57] X. X. Zhang, Y. You, S. Y. F. Zhao, and T. F. Heinz, "Experimental evidence for dark excitons in monolayer WSe<sub>2</sub>," Phys. Rev. Lett., vol. 115, no. 25, p. 257403, 2015.
- [58] Z. Ye, et al., "Probing excitonic dark states in single-layer tungsten disulphide," *Nature*, vol. 513, no. 7517, pp. 214-218, 2014.
- [59] C. Robert, et al., "Measurement of the spin-forbidden dark excitons in MoS<sub>2</sub> and MoSe<sub>2</sub> monolayers," Nat. Commun., vol. 11, no. 1, p. 4037, 2020.
- [60] J. Madéo, et al., "Directly visualizing the momentum-forbidden dark excitons and their dynamics in atomically thin semiconductors," Science, vol. 370, no. 6521, pp. 1199-1204, 2020.
- [61] E. C. Regan, et al., "Emerging exciton physics in transition metal dichalcogenide heterobilayers," Nat. Rev. Mater., vol. 7, no. 10, pp. 778-795, 2022.
- [62] T. Mueller and E. Malic, "Exciton physics and device application of two-dimensional transition metal dichalcogenide semiconductors," npj 2D Mater. Appl., vol. 2, no. 1, p. 29, 2018.
- [63] P. Merkl, et al., "Ultrafast transition between exciton phases in van der Waals heterostructures," Nat. Mater., vol. 18, no. 7, pp. 691 - 696, 2019.
- [64] M. Zimmerman, R. Rapaport, and S. Gazit, "Collective interlayer pairing and pair superfluidity in vertically stacked layers of dipolar excitons," Proc. Natl. Acad. Sci. U. S. A., vol. 119, no. 30, p. e2205845119, 2022.
- [65] D. Unuchek, A. Ciarrocchi, A. Avsar, K. Watanabe, T. Taniquchi, and A. Kis, "Room-temperature electrical control of exciton flux in a van der Waals heterostructure," Nature, vol. 560, no. 7718, pp. 340 - 344, 2018.
- [66] H. Guo, X. Zhang, and G. Lu, "Tuning moiré excitons in Janus heterobilayers for high-temperature Bose-Einstein condensation," Sci. Adv., vol. 8, no. 40, p. eabp9757, 2022.
- [67] Y. Shimazaki, I. Schwartz, K. Watanabe, T. Taniguchi, M. Kroner, and A. Imamoğlu, "Strongly correlated electrons and hybrid excitons in a moiré heterostructure," Nature, vol. 580, no. 7804, pp. 472-477, 2020.
- [68] F. Tagarelli, et al., "Electrical control of hybrid exciton transport in a van der Waals heterostructure," Nat. Photonics, vol. 17, no. 7, pp. 615 - 621, 2023.
- [69] E. M. Alexeev, et al., "Resonantly hybridized excitons in moiré superlattices in van der Waals heterostructures," Nature, vol. 567, no. 7746, pp. 81-86, 2019.
- [70] Y. Tang, et al., "Tuning layer-hybridized moiré excitons by the quantum-confined Stark effect," Nat. Nanotechnol., vol. 16, no. 1, pp. 52-57, 2021.
- [71] Y. Koo, et al., "Tunable interlayer excitons and switchable interlayer trions via dynamic near-field cavity," Light Sci. Appl., vol. 12, no. 1, p. 59, 2023.

- [72] C. Choi, et al., "Enhanced interlayer neutral excitons and trions in trilayer van der Waals heterostructures," npj 2D Mater. Appl., vol. 2, no. 1, p. 30, 2018.
- [73] E. Calman, et al., "Indirect excitons and trions in MoSe<sub>2</sub>/WSe<sub>2</sub> van der Waals heterostructures," Nano Lett., vol. 20, no. 3, pp. 1869-1875, 2020.
- [74] L. Zhang, et al., "Discovery of type II interlayer trions," Adv. Mater., vol. 35, no. 5, p. 2206212, 2023.
- [75] M. Kremser, et al., "Discrete interactions between a few interlayer excitons trapped at a MoSe<sub>2</sub> – WSe<sub>2</sub> heterointerface," npj 2D Mater. Appl., vol. 4, no. 1, p. 8, 2020.
- [76] W. Li, X. Lu, S. Dubey, L. Devenica, and A. Srivastava, "Dipolar interactions between localized interlayer excitons in van der Waals heterostructures," Nat. Mater., vol. 19, no. 6, pp. 624-629,
- [77] X. Sun, et al., "Enhanced interactions of interlayer excitons in free-standing heterobilayers," Nature, vol. 610, no. 7932, pp. 478-484, 2022.
- [78] K. Hao, et al., "Neutral and charged inter-valley biexcitons in monolayer MoSe<sub>2</sub>," Nat. Commun., vol. 8, no. 1, p. 15552, 2017.
- [79] Z. Li, et al., "Revealing the biexciton and trion-exciton complexes in BN encapsulated WSe<sub>2</sub>," Nat. Commun., vol. 9, no. 1, p. 3719,
- [80] E. Y. Andrei, et al., "The marvels of moiré materials," Nat. Rev. Mater., vol. 6, no. 3, pp. 201-206, 2021.
- [81] K. F. Mak and J. Shan, "Semiconductor moiré materials," Nat. *Nanotechnol.*, vol. 17, no. 7, pp. 686 – 695, 2022.
- [82] X. Wang, et al., "Moiré trions in MoSe<sub>2</sub>/WSe<sub>2</sub> heterobilayers," Nat. Nanotechnol., vol. 16, no. 11, pp. 1208-1213, 2021.
- [83] E. Liu, et al., "Signatures of moiré trions in WSe<sub>2</sub>/MoSe<sub>2</sub> heterobilayers," Nature, vol. 594, no. 7861, pp. 46-50, 2021.
- [84] K. Tran, et al., "Evidence for moiré excitons in van der Waals heterostructures," *Nature*, vol. 567, no. 7746, pp. 71-75, 2019.
- [85] C. Jin, et al., "Observation of moiré excitons in WSe<sub>2</sub>/WS<sub>2</sub> heterostructure superlattices," Nature, vol. 567, no. 7746, pp.
- [86] K. L. Seyler, et al., "Signatures of moiré-trapped valley excitons in MoSe<sub>2</sub>/WSe<sub>2</sub> heterobilayers," Nature, vol. 567, no. 7746, pp. 66 - 70, 2019.
- [87] N. P. Wilson, W. Yao, J. Shan, and X. Xu, "Excitons and emergent quantum phenomena in stacked 2D semiconductors," Nature, vol. 599, no. 7885, pp. 383-392, 2021.
- [88] L. Du, M. R. Molas, Z. Huang, G. Zhang, F. Wang, and Z. Sun, "Moiré photonics and optoelectronics," Science, vol. 379, no. 6639, p. eadg0014, 2023.
- [89] L. Zhao, Q. Shang, M. Li, Y. Liang, C. Li, and Q. Zhang, "Strong exciton-photon interaction and lasing of two-dimensional transition metal dichalcogenide semiconductors," Nano Res., vol. 14, no. 14, pp. 1937-1954, 2021.
- [90] C. F. Klingshirn, Semiconductor Optics, Springer Science & Business Media, 2012.
- [91] J. Zhang, W. Zhao, P. Yu, G. Yang, and Z. Liu, "Second harmonic generation in 2D layered materials," 2D Mater., vol. 7, no. 4, p. 042002, 2020.
- [92] J. A. Schuller, et al., "Orientation of luminescent excitons in layered nanomaterials," Nat. Nanotechnol., vol. 8, no. 4, pp.
- [93] D. Xiao, G. B. Liu, W. Feng, X. Xu, and W. Yao, "Coupled spin and valley physics in monolayers of MoS<sub>2</sub> and other group-VI

- dichalcogenides," Phys. Rev. Lett., vol. 108, no. 19, p. 196802,
- [94] T. Cao, et al., "Valley-selective circular dichroism of monolayer molybdenum disulphide," Nat. Commun., vol. 3, no. 1, p. 887, 2012.
- [95] J. Kim, et al., "Ultrafast generation of pseudo-magnetic field for valley excitons in WSe<sub>2</sub> monolayers," Science, vol. 346, no. 6214, pp. 1205-1208, 2014.
- [96] A. M. Jones, et al., "Spin—layer locking effects in optical orientation of exciton spin in bilayer WSe<sub>2</sub>," Nat. Phys., vol. 10, no. 2, pp. 130-134, 2014.
- [97] J. Zhang, et al., "Enhancing and controlling valley magnetic response in MoS<sub>2</sub>/WS<sub>2</sub> heterostructures by all-optical route," Nat. Commun., vol. 10, no. 1, p. 4226, 2019.
- [98] J. R. Schaibley, et al., "Valleytronics in 2D materials," Nat. Rev. Mater., vol. 1, no. 11, p. 16055, 2016.
- [99] W. Yang, et al., "Electrically tunable valley-light emitting diode (vLED) based on CVD-grown monolayer WS2," Nano Lett., vol. 16, no. 3, pp. 1560-1567, 2016.
- [100] S. Feng, et al., "Engineering valley polarization of monolayer WS<sub>2</sub>: a physical doping approach," Small, vol. 15, no. 12, p. 1805503,
- [101] X. Cui, et al., "Multi-terminal transport measurements of MoS<sub>2</sub> using a van der Waals heterostructure device platform," Nat. Nanotechnol., vol. 10, no. 6, pp. 534-540, 2015.
- [102] K. Kang, et al., "High-mobility three-atom-thick semiconducting films with wafer-scale homogeneity," Nature, vol. 520, no. 7549, pp. 656-660, 2015.
- [103] Y. Liu, et al., "Room temperature nanocavity laser with interlayer excitons in 2D heterostructures," Sci. Adv., vol. 5, no. 4, p. eaay4506, 2019.
- [104] E. Y. Paik, L. Zhang, G. W. Burg, R. Gogna, E. Tutuc, and H. Deng, "Interlayer exciton laser of extended spatial coherence in atomically thin heterostructures," Nature, vol. 576, no. 7785, pp. 80 - 84.2019.
- [105] O. Salehzadeh, M. Djavid, N. H. Tran, I. Shih, and Z. Mi, "Optically pumped two-dimensional MoS2 lasers operating at room-temperature," *Nano Lett.*, vol. 15, no. 8, pp. 5302-5306,
- [106] Y. Ye, et al., "Monolayer excitonic laser," Nat. Photonics, vol. 9, no. 11, pp. 733-737, 2015.
- [107] Y. Li, et al., "Room-temperature continuous-wave lasing from monolayer molybdenum ditelluride integrated with a silicon nanobeam cavity," Nat. Nanotechnol., vol. 12, no. 10, pp. 987-992,
- [108] J. Shang, et al., "Room-temperature 2D semiconductor activated vertical-cavity surface-emitting lasers," Nat. Commun., vol. 8, no. 1, p. 543, 2017.
- [109] L. Zhao, et al., "High-temperature continuous-wave pumped lasing from large-area monolayer semiconductors grown by chemical vapor deposition," ACS Nano, vol. 12, no. 9, pp. 9390-9396, 2018.
- [110] K. Rong, et al., "Spin-valley Rashba monolayer laser," Nat. Mater., vol. 22, no. 9, pp. 1085-1093, 2023.
- [111] C. Qian, et al., "Lasing of moiré trapped MoSe<sub>2</sub>/WSe<sub>2</sub> interlayer excitons coupled to a nanocavity," Sci. Adv., vol. 10, no. 2, p. eadk6359, 2024.
- [112] J. Sung, et al., "Room-temperature continuous-wave indirect-bandgap transition lasing in an ultra-thin WS<sub>2</sub> disk," Nat. Photonics, vol. 16, no. 11, pp. 792-797, 2022.

- [113] S. Strauf and F. Jahnke, "Single quantum dot nanolaser," Laser Photonics Rev., vol. 5, no. 5, pp. 607-633, 2011.
- [114] R. F. Oulton, et al., "Plasmon lasers at deep subwavelength scale," Nature, vol. 461, no. 7264, pp. 629-632, 2009.
- [115] O. Painter, et al., "Two-dimensional photonic band-gap defect mode laser," Science, vol. 284, no. 5421, pp. 1819 – 1821, 1999.
- [116] M. Khajavikhan, et al., "Thresholdless nanoscale coaxial lasers," *Nature*, vol. 482, no. 7384, pp. 204-207, 2012.
- [117] S. Strauf, et al., "Self-tuned quantum dot gain in photonic crystal lasers," Phys. Rev. Lett., vol. 96, no. 12, p. 127404, 2006.
- [118] M. A. Green and M. J. Keevers, "Optical properties of intrinsic silicon at 300 K," Prog. Photovoltaics Res. Appl., vol. 3, no. 3, pp. 189-192, 1995.
- [119] R. Hull, Properties of Crystalline Silicon, London, INSPEC, 1999.
- [120] A. Ramasubramaniam, "Large excitonic effects in monolayers of molybdenum and tungsten dichalcogenides," Phys. Rev. B, vol. 86, no. 11, p. 115409, 2012.
- [121] C. Ruppert, B. Aslan, and T. F. Heinz, "Optical properties and band gap of single- and few-layer MoTe<sub>2</sub> crystals," Nano Lett., vol. 14, no. 11, pp. 6231-6236, 2014.
- [122] G. Christmann, R. Butté, E. Feltin, J. F. Carlin, and N. Grandjean, "Room temperature polariton lasing in a GaN/AlGaN multiple quantum well microcavity," Appl. Phys. Lett., vol. 93, no. 5, p. 051102, 2008.
- [123] S. L. McCall, A. F. J. Levi, R. E. Slusher, S. J. Pearton, and R. A. Logan, "Whispering-gallery mode microdisk lasers," Appl. Phys. Lett., vol. 60, no. 3, pp. 289 – 291, 1992.
- [124] J. H. Wade and R. C. Bailey, "Applications of optical microcavity resonators in analytical chemistry," Annu. Rev. Anal. Chem., vol. 9, pp. 1-25, 2016.
- [125] N. Toropov, G. Cabello, M. P. Serrano, R. R. Gutha, M. Rafti, and F. Vollmer, "Review of biosensing with whispering-gallery mode lasers," Light Sci. Appl., vol. 10, no. 1, p. 42, 2021.
- [126] M. C. Houghton, S. V. Kashanian, T. L. Derrien, K. Masuda, and F. Vollmer, "Whispering-gallery mode optoplasmonic microcavities: from advanced single-molecule sensors and microlasers to applications in synthetic biology," ACS Photonics, vol. 11, no. 3, pp. 892 - 903, 2024.
- [127] Y. Wang, S. Zeng, G. Humbert, and H. Ho, "Microfluidic whispering gallery mode optical sensors for biological applications," Laser Photonics Rev., vol. 14, no. 12, p. 2000135, 2020.
- [128] Y. Mi, et al., "Tuning excitonic properties of monolayer MoS<sub>2</sub> with microsphere cavity by high-throughput chemical vapor deposition method," Small, vol. 13, no. 42, p. 1701694, 2017.
- [129] G. Berghäuser and E. Malic, "Analytical approach to excitonic properties of MoS<sub>2</sub>," Phys. Rev. B, vol. 89, no. 12, p. 125309, 2014.
- M. Florian, et al., "The dielectric impact of layer distances on exciton and trion binding energies in van der Waals heterostructures," Nano Lett., vol. 18, no. 4, pp. 2725-2732, 2018.
- [131] L. Reeves, Y. Wang, and T. F. Krauss, "2D material microcavity light emitters: to lase or not to lase?," Adv. Opt. Mater., vol. 6, no. 19, p. 1800272, 2018.
- [132] H. Fang, et al., "Strong interlayer coupling in van der Waals heterostructures built from single-layer chalcogenides," Proc. Natl. Acad. Sci. U. S. A., vol. 111, no. 17, pp. 6198 – 6202, 2014.
- [133] L. Zhang, R. Gogna, W. Burg, E. Tutuc, and H. Deng, "Photonic-crystal exciton-polaritons in monolayer semiconductors," Nat. Commun., vol. 9, no. 1, p. 713, 2018.

- [134] L. Zhang, et al., "Highly valley-polarized singlet and triplet interlayer excitons in van der Waals heterostructure," Phys. Rev. B. vol. 100, no. 4, p. 041402, 2019.
- [135] C. H. Lee, et al., "Atomically thin p-n junctions with van der Waals heterointerfaces," Nat. Nanotechnol., vol. 9, no. 9, pp. 676-681, 2014.
- [136] J. S. Ross, et al., "Interlayer exciton optoelectronics in a 2D heterostructure p-n junction," Nano Lett., vol. 17, no. 2, pp.
- [137] F. Xia, H. Wang, D. Xiao, M. Dubey, and A. Ramasubramaniam, "Two-dimensional material nanophotonics," Nat. Photonics, vol. 8, no. 12, pp. 899-907, 2014.
- [138] K. F. Mak and J. Shan, "Photonics and optoelectronics of 2D semiconductor transition metal dichalcogenides," Nat. Photonics, vol. 10, no. 4, pp. 216-226, 2016.
- [139] H. Yu, G.-B. Liu, J. Tang, X. Xu, and W. Yao, "Moiré excitons: from programmable quantum emitter arrays to spin-orbit - coupled artificial lattices," Sci. Adv., vol. 3, no. 11, p. e1701696, 2017.
- [140] H. Baek, et al., "Highly energy-tunable quantum light from moiré-trapped excitons," Sci. Adv., vol. 6, no. 37, p. eaba8526,
- [141] Y. Jiang, S. Chen, W. Zheng, B. Zheng, and A. Pan, "Interlayer exciton formation, relaxation, and transport in TMD van der Waals heterostructures," Light Sci. Appl., vol. 10, no. 1, p. 72, 2021.
- [142] G. Cao, et al., "2D material based synaptic devices for neuromorphic computing," Adv. Funct. Mater., vol. 31, no. 4, p. 2005443, 2021.
- [143] D. A. Bandurin, et al., "High electron mobility, quantum Hall effect and anomalous optical response in atomically thin InSe," Nat. Nanotechnol., vol. 12, no. 3, pp. 223-227, 2017.
- [144] T. Shubina, et al., "InSe as a case between 3D and 2D layered crystals for excitons," Nat. Commun., vol. 10, no. 1, p. 3479, 2019.
- [145] M. Brotons-Gisbert, et al., "Nanotexturing to enhance photoluminescent response of atomically thin indium selenide with highly tunable band gap," Nano Lett., vol. 16, no. 5, pp. 3221 - 3229, 2016.
- [146] G. W. Mudd, et al., "Tuning the bandgap of exfoliated InSe nanosheets by quantum confinement," Adv. Mater., vol. 25, no. 40, p. 5714, 2013.
- [147] M. Brotons-Gisbert, et al., "Out-of-plane orientation of luminescent excitons in two-dimensional indium selenide," Nat. Commun., vol. 10, no. 1, p. 3913, 2019.
- [148] L. He, Ş. K. Özdemir, and L. Yang, "Whispering gallery microcavity lasers," *Laser Photonics Rev.*, vol. 7, no. 1, pp. 60 – 82, 2013.
- [149] R. M. Ma and R. F. Oulton, "Applications of nanolasers," Nat. Nanotechnol., vol. 14, no. 1, pp. 12-22, 2019.
- [150] J. B. Khurgin and G. Sun, "Comparative analysis of spasers, vertical-cavity surface-emitting lasers and surface-plasmon-emitting diodes," Nat. Photonics, vol. 8, no. 6, pp. 468-473, 2014.
- [151] L. Zhao, et al., "Engineering near-infrared light emission in mechanically exfoliated InSe platelets through hydrostatic pressure for multicolor microlasing," Nano Lett., vol. 22, no. 9, pp. 3840-3847, 2022.
- [152] C. Weisbuch, M. Nishioka, A. Ishikawa, and Y. Arakawa, "Observation of the coupled exciton-photon mode splitting in a semiconductor quantum microcavity," Phys. Rev. Lett., vol. 69, no. 23, p. 3314, 1992.

- [153] J. Kasprzak, et al., "Bose Einstein condensation of exciton polaritons," *Nature*, vol. 443, no. 7110, pp. 409 – 414, 2006.
- [154] R. Balili, V. Hartwell, D. Snoke, L. Pfeiffer, and K. West, "Bose - Einstein condensation of microcavity polaritons in a trap," Science, vol. 316, no. 5827, pp. 1007-1010, 2007.
- [155] H. Deng, H. Haug, and Y. Yamamoto, "Exciton-polariton Bose - Einstein condensation," Rev. Mod. Phys., vol. 82, no. 2, pp. 1489 - 1537, 2010.
- [156] H. Deng, G. Weihs, D. Snoke, J. Bloch, and Y. Yamamoto, "Polariton lasing vs. photon lasing in a semiconductor microcavity," Proc. Natl. Acad. Sci. U. S. A., vol. 100, no. 26, pp. 15318-15323, 2003.
- [157] P. Savvidis, J. Baumberg, R. Stevenson, M. S. Skolnick, D. M. Whittaker, and J. S. Roberts, "Angle-resonant stimulated polariton amplifier," Phys. Rev. Lett., vol. 84, no. 7, p. 1547, 2000.
- [158] A. Amo, et al., "Exciton—polariton spin switches," Nat. Photonics, vol. 4, no. 6, pp. 361-366, 2010.
- [159] W. Zhou, et al., "Progress in 2D photonic crystal Fano resonance photonics," Prog. Quantum Electron., vol. 38, no. 1, pp. 1-74, 2014.
- [160] A. E. Miroshnichenko, S. Flach, and Y. S. Kivshar, "Fano resonances in nanoscale structures," Rev. Mod. Phys., vol. 82, no. 3, pp. 2257-2298, 2010.
- [161] S. Christopoulos, et al., "Room-temperature polariton lasing in semiconductor microcavities," Phys. Rev. Lett., vol. 98, no. 12, p. 126405, 2007.
- [162] D. Bajoni, et al., "Polariton laser using single micropillar GaAs-GaAlAs semiconductor cavities," Phys. Rev. Lett., vol. 100, no. 4. p. 047401, 2008.
- [163] J. Zhao, et al., "Ultralow threshold polariton condensate in a monolayer semiconductor microcavity at room temperature," Nano Lett., vol. 21, no. 7, pp. 3331-3339, 2021.
- [164] Y. J. Chen, J. D. Cain, T. K. Stanev, V. P. Dravid, and N. P. Stern, "Valley-polarized exciton – polaritons in a monolayer semiconductor," Nat. Photonics, vol. 11, no. 7, pp. 431-435, 2017.
- [165] Z. Sun, et al., "Optical control of room-temperature valley polaritons," *Nat. Photonics*, vol. 11, no. 8, pp. 491 – 496, 2017.
- [166] L. Qiu, C. Chakraborty, S. Dhara, and A. N. Vamivakas, "Room-temperature valley coherence in a polaritonic system," Nat. Commun., vol. 10, no. 1, p. 1513, 2019.
- [167] A. Imamog, R. Ram, S. Pau, and Y. Yamamoto, "Nonequilibrium condensates and lasers without inversion: exciton-polariton lasers," Phys. Rev. A, vol. 53, no. 6, p. 4250, 1996.
- [168] M. D. Fraser, S. Höfling, and Y. Yamamoto, "Physics and applications of exciton - polariton lasers," Nat. Mater., vol. 15, no. 10, pp. 1049-1052, 2016.
- [169] A. G. Del Águila, et al., "Ultrafast exciton fluid flow in an atomically thin MoS<sub>2</sub> semiconductor," Nat. Nanotechnol., vol. 18, no. 9, pp. 1012-1019, 2023.
- [170] J. Zhao, et al., "Exciton polariton interactions in Van der Waals superlattices at room temperature," Nat. Commun., vol. 14, no. 1, p. 1512, 2023.
- [171] D. Schmidt, et al., "Tracking dark excitons with exciton polaritons in semiconductor microcavities," Phys. Rev. Lett., vol. 122, no. 4, p. 047403, 2019.
- [172] H. Cho, D. J. Shin, J. Sung, and S. H. Gong, "Ultra-thin grating coupler for guided exciton-polaritons in WS2 multilayers," Nanophotonics, vol. 12, no. 13, pp. 2563 – 2571, 2023.

- [173] X. Zhang, et al., "Ultrathin WS2-on-glass photonic crystal for self-resonant exciton-polaritonics," Adv. Opt. Mater., vol. 8, no. 7, p. 1901988, 2020.
- [174] D. J. Shin, H. Cho, J. Sung, and S. Gong, "Direct observation of self-hybridized exciton-polaritons and their valley polarizations in a bare WS2 layer," Adv. Mater., vol. 34, no. 50, p. 2207735, 2022.
- [175] J. Beck, "Über chalkogenidhalogenide des chroms synthese, kristallstruktur und magnetismus von chromsulfidbromid, CrSBr," Z. Anorg. Allg. Chem., vol. 585, no. 1, pp. 157-167, 1990.
- [176] O. Göser, W. Paul, and H. Kahle, "Magnetic properties of CrSBr," J. Magn. Magn. Mater., vol. 92, no. 1, pp. 129-136, 1990.
- [177] E. J. Telford, et al., "Layered antiferromagnetism induces large negative magnetoresistance in the van der Waals semiconductor CrSBr," Adv. Mater., vol. 32, no. 37, p. 2003240, 2020.
- [178] K. Yang, G. Wang, L. Liu, D. Lu, and H. Wu, "Triaxial magnetic anisotropy in the two-dimensional ferromagnetic semiconductor CrSBr," Phys. Rev. B, vol. 104, no. 14, p. 144416, 2021.
- [179] N. P. Wilson, et al., "Interlayer electronic coupling on demand in a 2D magnetic semiconductor," Nat. Mater., vol. 20, no. 12, pp. 1657-1662, 2021.
- [180] K. Lee, et al., "Magnetic order and symmetry in the 2D semiconductor CrSBr," Nano Lett., vol. 21, no. 8, pp. 3511-3517, 2021.
- [181] F. Dirnberger, et al., "Magneto-optics in a van der Waals magnet tuned by self-hybridized polaritons," Nature, vol. 620, no. 7974, pp. 533-537, 2023.
- [182] T. Wang, et al., "Magnetically-dressed CrSBr exciton-polaritons in ultrastrong coupling regime," Nat. Commun., vol. 14, no. 1, p. 5966, 2023.
- [183] N. Gisin and R. Thew, "Quantum communication," Nat. Photonics, vol. 1, no. 3, pp. 165-171, 2007.
- [184] E. Knill, R. Laflamme, and G. J. Milburn, "A scheme for efficient quantum computation with linear optics," Nature, vol. 409, no. 6816, pp. 46-52, 2001.
- [185] J. L. O'brien, "Optical quantum computing," Science, vol. 318, no. 5856, pp. 1567—1570, 2007.
- [186] M. Müller, et al., "Quantum-dot single-photon sources for entanglement enhanced interferometry," Phys. Rev. Lett., vol. 118, no. 25, p. 257402, 2017.
- [187] J. Klein, et al., "Site-selectively generated photon emitters in monolayer MoS2 via local helium ion irradiation," Nat. Commun., vol. 10, no. 1, p. 2755, 2019.
- [188] K. Parto, S. I. Azzam, K. Banerjee, and G. Moody, "Defect and strain engineering of monolayer WSe2 enables site-controlled single-photon emission up to 150 K," Nat. Commun., vol. 12, no. 1, p. 3585, 2021.
- [189] H. Ngoc My Duong, et al., "Effects of high-energy electron irradiation on quantum emitters in hexagonal boron nitride," ACS *Appl. Mater. Interfaces*, vol. 10, no. 29, pp. 24886 – 24891, 2018.
- [190] C. Fournier, et al., "Position-controlled quantum emitters with reproducible emission wavelength in hexagonal boron nitride," Nat. Commun., vol. 12, no. 1, p. 3779, 2021.
- [191] Y. Chen, et al., "Generation of high-density quantum emitters in high-quality, exfoliated hexagonal boron nitride," ACS Appl. Mater. Interfaces, vol. 13, no. 39, pp. 47283-47292, 2021.
- [192] A. Scavuzzo, et al., "Electrically tunable quantum emitters in an ultrathin graphene – hexagonal boron nitride van der Waals heterostructure," Appl. Phys. Lett., vol. 114, no. 6, 2019. https://doi .org/10.1063/1.5067385.

- [193] N. V. Proscia, et al., "Microcavity-coupled emitters in hexagonal boron nitride," Nanophotonics, vol. 9, no. 9, pp. 2937-2944, 2020.
- [194] J. E. Fröch, S. Kim, N. Mendelson, M. Kianinia, M. Toth, and I. Aharonovich, "Coupling hexagonal boron nitride quantum emitters to photonic crystal cavities," ACS Nano, vol. 14, no. 6, pp. 7085 - 7091, 2020.
- [195] L. C. Flatten, et al., "Microcavity enhanced single photon emission from two-dimensional WSe2," Appl. Phys. Lett., vol. 112, no. 19, 2018. https://doi.org/10.1063/1.5026779.
- [196] A. Hötger, et al., "Gate-switchable arrays of quantum light emitters in contacted monolayer MoS2 van der Waals heterodevices," Nano Lett., vol. 21, no. 2, pp. 1040-1046, 2021.
- [197] C. A. Chen, et al., "Tunable single-photon emission with wafer-scale plasmonic array," Nano Lett., vol. 24, no. 11, pp. 3395-3403 2024
- [198] P. Senellart, G. Solomon, and A. White, "High-performance semiconductor quantum-dot single-photon sources," Nat. Nanotechnol., vol. 12, no. 11, pp. 1026-1039, 2017.
- [199] S. Sempere-Llagostera, G. Thekkadath, R. Patel, W. S. Kolthammer, and I. A. Walmsley, "Reducing g<sup>(2)</sup>(0) of a parametric down-conversion source via photon-number resolution with superconducting nanowire detectors," Opt. Express, vol. 30, no. 2, pp. 3138 – 3147, 2022.
- [200] S. I. Davis, et al., "Improved heralded single-photon source with a photon-number-resolving superconducting nanowire detector," Phys. Rev. Appl., vol. 18, no. 6, p. 064007, 2022.
- [201] N. Tomm, et al., "A bright and fast source of coherent single photons," Nat. Nanotechnol., vol. 16, no. 4, pp. 399-403, 2021.
- [202] X. Ding, et al., "High-efficiency single-photon source above the loss-tolerant threshold for efficient linear optical quantum computing," arXiv preprint arXiv:2311.08347, 2023.
- [203] R. Uppu, et al., "Scalable integrated single-photon source," Sci. Adv., vol. 6, no. 50, p. eabc8268, 2020.
- [204] N. Somaschi, et al., "Near-optimal single-photon sources in the solid state," *Nat. Photonics*, vol. 10, no. 5, pp. 340 – 345, 2016.
- [205] X. Ding, et al., "On-demand single photons with high extraction efficiency and near-unity indistinguishability from a resonantly driven quantum dot in a micropillar," Phys. Rev. Lett., vol. 116, no. 2, p. 020401, 2016.
- [206] S. Unsleber, et al., "Highly indistinguishable on-demand resonance fluorescence photons from a deterministic quantum dot micropillar device with 74% extraction efficiency," Opt. Express, vol. 24, no. 8, pp. 8539 – 8546, 2016.
- [207] M. Atatüre, D. Englund, N. Vamivakas, S. Y. Lee, and J. Wrachtrup, "Material platforms for spin-based photonic quantum technologies," *Nat. Rev. Mater.*, vol. 3, no. 5, pp. 38-51, 2018.
- [208] D. Chen, N. Zheludev, and W. B. Gao, "Building blocks for quantum network based on group-IV split-vacancy centers in diamond," Adv. Quantum Technol., vol. 3, no. 2, p. 1900069, 2020.
- [209] S. Castelletto, "Silicon carbide single-photon sources: challenges and prospects," Mater. Quantum Technol., vol. 1, no. 2, p. 023001, 2021.
- [210] P. K. Shandilya, et al., "Diamond integrated quantum nanophotonics: spins, photons and phonons," J. Lightwave Technol., vol. 40, no. 23, pp. 7538 – 7571, 2022.
- [211] M. Koperski, et al., "Single photon emitters in exfoliated WSe<sub>2</sub> structures," Nat. Nanotechnol., vol. 10, no. 6, pp. 503-506, 2015.
- [212] C. Chakraborty, L. Kinnischtzke, K. M. Goodfellow, R. Beams, and A. N. Vamivakas, "Voltage-controlled quantum light from an

- atomically thin semiconductor," Nat. Nanotechnol., vol. 10, no. 6, pp. 507-511, 2015.
- [213] R. Schmidt, et al., "Reversible uniaxial strain tuning in atomically thin WSe<sub>2</sub>," 2D Mater., vol. 3, no. 2, p. 021011, 2016.
- [214] L. Sortino, et al., "Bright single photon emitters with enhanced quantum efficiency in a two-dimensional semiconductor coupled with dielectric nano-antennas," Nat. Commun., vol. 12, no. 1, p. 6063, 2021.
- [215] F. Hayee, et al., "Revealing multiple classes of stable quantum emitters in hexagonal boron nitride with correlated optical and electron microscopy," Nat. Mater., vol. 19, no. 5, pp. 534-539, 2020.
- [216] C. Jara, et al., "First-principles identification of single photon emitters based on carbon clusters in hexagonal boron nitride," J. Phys. Chem. A, vol. 125, no. 6, pp. 1325-1335, 2021.
- [217] Q. Tan, et al., "Donor-acceptor pair quantum emitters in hexagonal boron nitride," Nano Lett., vol. 22, no. 3, pp. 1331-1337, 2022.
- [218] O. Golami, et al., "Ab initio and group theoretical study of properties of a carbon trimer defect in hexagonal boron nitride," Phys. Rev. B, vol. 105, no. 18, p. 184101, 2022.
- [219] M. Abdi, J. P. Chou, A. Gali, and M. B. Plenio, "Color centers in hexagonal boron nitride monolayers: a group theory and ab initio analysis," ACS Photonics, vol. 5, no. 5, pp. 1967—1976, 2018.
- [220] P. Auburger and A. Gali, "Towards ab initio identification of paramagnetic substitutional carbon defects in hexagonal boron nitride acting as quantum bits," Phys. Rev. B, vol. 104, no. 7, p. 075410, 2021.
- [221] K. Li, T. J. Smart, and Y. Ping, "Carbon trimer as a 2 eV single-photon emitter candidate in hexagonal boron nitride: a first-principles study," Phys. Rev. Mater., vol. 6, no. 4, p. L042201,
- [222] V. Ivády, et al., "Ab initio theory of the negatively charged boron vacancy qubit in hexagonal boron nitride," npj Comput. Mater., vol. 6, no. 1, p. 41, 2020.
- [223] S. Li, A. Pershin, G. Thiering, P. Udvarhelyi, and A. Gali, "Ultraviolet quantum emitters in hexagonal boron nitride from carbon clusters," J. Phys. Chem. Lett., vol. 13, no. 14, pp. 3150-3157,
- [224] Á. Ganvecz, R. Babar, Z. Benedek, I. Aharonovich, G. Barcza, and V. Ivády, "First-principles theory of the nitrogen interstitial in hBN: a plausible model for the blue emitter," Nanoscale, vol. 16, no. 8, pp. 4125-4139, 2024.
- [225] A. Branny, S. Kumar, R. Proux, and B. D. Gerardot, "Deterministic strain-induced arrays of quantum emitters in a two-dimensional semiconductor," Nat. Commun., vol. 8, no. 1, p. 15053, 2017.
- [226] O. Iff, et al., "Strain-tunable single photon sources in WSe<sub>2</sub> monolayers," Nano Lett., vol. 19, no. 10, pp. 6931-6936, 2019.
- [227] S. Choi, et al., "Engineering and localization of quantum emitters in large hexagonal boron nitride layers," ACS Appl. Mater. Interfaces, vol. 8, no. 43, pp. 29642-29648, 2016.
- [228] T. T. Tran, et al., "Robust multicolor single photon emission from point defects in hexagonal boron nitride," ACS Nano, vol. 10, no. 8, pp. 7331-7338, 2016.
- [229] G. Grosso, et al., "Tunable and high-purity room temperature single-photon emission from atomic defects in hexagonal boron nitride," Nat. Commun., vol. 8, no. 1, p. 705, 2017.
- [230] D. A. Harmin, "Theory of the Stark effect," Phys. Rev. A, vol. 26, no. 5, p. 2656, 1982.

- [231] C. Chakraborty, K. M. Goodfellow, S. Dhara, A. Yoshimura, V. Meunier, and A. N. Vamivakas, "Quantum-confined Stark effect of individual defects in a van der Waals heterostructure," Nano Lett., vol. 17, no. 4, pp. 2253-2258, 2017.
- [232] G. Noh, et al., "Stark tuning of single-photon emitters in hexagonal boron nitride," Nano Lett., vol. 18, no. 8, pp. 4710 - 4715, 2018.
- [233] Y. Xia, et al., "Room-temperature giant Stark effect of single photon emitter in van der Waals material," Nano Lett., vol. 19, no. 10, pp. 7100-7105, 2019.
- [234] A. M. Jones, et al., "Optical generation of excitonic valley coherence in monolayer WSe2," Nat. Nanotechnol., vol. 8, no. 9, pp. 634-638, 2013.
- [235] D. Gammon, E. Snow, B. Shanabrook, D. S. Katzer, and D. Park, "Fine structure splitting in the optical spectra of single GaAs quantum dots," Phys. Rev. Lett., vol. 76, no. 16, p. 3005, 1996.
- [236] O. Iff, et al., "Purcell-enhanced single photon source based on a deterministically placed WSe<sub>2</sub> monolayer quantum dot in a circular Bragg grating cavity," Nano Lett., vol. 21, no. 11, pp. 4715-4720, 2021.
- [237] M. Blauth, et al., "Coupling single photons from discrete quantum emitters in WSe2 to lithographically defined plasmonic slot waveguides," Nano Lett., vol. 18, no. 11, pp. 6812-6819, 2018.
- [238] J. Wierzbowski, et al., "Direct exciton emission from atomically thin transition metal dichalcogenide heterostructures near the lifetime limit," Sci. Rep., vol. 7, no. 1, p. 12383, 2017.
- [239] O. A. Ajayi, et al., "Approaching the intrinsic photoluminescence linewidth in transition metal dichalcogenide monolayers," 2D Mater., vol. 4, no. 3, p. 031011, 2017.
- [240] F. Cadiz, et al., "Excitonic linewidth approaching the homogeneous limit in MoS<sub>2</sub>-based van der Waals heterostructures," Phys. Rev. X, vol. 7, no. 2, p. 021026, 2017.
- [241] P. Tonndorf, et al., "Single-photon emission from localized excitons in an atomically thin semiconductor," Optica, vol. 2, no. 4, pp. 347-352, 2015.
- [242] F. Peyskens, C. Chakraborty, M. Muneeb, D. Van Thourhout, and D. Englund, "Integration of single photon emitters in 2D layered materials with a silicon nitride photonic chip," Nat. Commun., vol. 10, no. 1, p. 4435, 2019.
- [243] N. Mendelson, et al., "Engineering and tuning of quantum emitters in few-layer hexagonal boron nitride," ACS Nano, vol. 13, no. 3, pp. 3132-3140, 2019.
- [244] A. L. Exarhos, D. A. Hopper, R. R. Grote, A. Alkauskas, and L. C. Bassett, "Optical signatures of quantum emitters in suspended hexagonal boron nitride," ACS Nano, vol. 11, no. 3, pp. 3328 - 3336, 2017.
- [245] N. R. Jungwirth, B. Calderon, Y. Ji, M. G. Spencer, M. E. Flatté, and G. D. Fuchs, "Temperature dependence of wavelength selectable zero-phonon emission from single defects in hexagonal boron nitride," Nano Lett., vol. 16, no. 10, pp. 6052-6057, 2016.
- [246] N. V. Proscia, et al., "Near-deterministic activation of room-temperature quantum emitters in hexagonal boron nitride," Optica, vol. 5, no. 9, pp. 1128-1134, 2018.
- [247] A. W. Schell, H. Takashima, T. T. Tran, I. Aharonovich, and S. Takeuchi, "Coupling quantum emitters in 2D materials with tapered fibers," ACS Photonics, vol. 4, no. 4, pp. 761-767, 2017.
- [248] S. Kim, et al., "Integrated on chip platform with quantum emitters in layered materials," Adv. Opt. Mater., vol. 7, no. 23, p. 1901132, 2019.

- [249] C. Errando-Herranz, et al., "Resonance fluorescence from waveguide-coupled, strain-localized, two-dimensional guantum emitters," ACS Photonics, vol. 8, no. 4, pp. 1069-1076, 2021.
- [250] Z. Sun, A. Martinez, and F. Wang, "Optical modulators with 2D layered materials," Nat. Photonics, vol. 10, no. 4, pp. 227-238,
- [251] M. Ono, et al., "Ultrafast and energy-efficient all-optical switching with graphene-loaded deep-subwavelength plasmonic waveguides," Nat. Photonics, vol. 14, no. 1, pp. 37-43, 2020.
- [252] N. Tancogne-Dejean, O. D. Mücke, F. X. Kärtner, and A. Rubio, "Impact of the electronic band structure in high-harmonic generation spectra of solids," Phys. Rev. Lett., vol. 118, no. 8, p.
- [253] S. Shree, et al., "Interlayer exciton mediated second harmonic generation in bilayer MoS2," Nat. Commun., vol. 12, no. 1, p. 6894, 2021.
- [254] R. Ma, D. S. Sutherland, and Y. Shi, "Harmonic generation in transition metal dichalcogenides and their heterostructures," Mater. Today, vol. 50, pp. 570-586, 2021.
- [255] A. R. Khan, et al., "Optical harmonic generation in 2D materials," Adv. Funct. Mater., vol. 32, no. 3, p. 2105259, 2022.
- [256] A. Säynätjoki, et al., "Ultra-strong nonlinear optical processes and trigonal warping in MoS<sub>2</sub> layers," Nat. Commun., vol. 8, no. 1, p. 893, 2017.
- [257] Y. Li, et al., "Probing symmetry properties of few-layer MoS<sub>2</sub> and h-BN by optical second-harmonic generation," Nano Lett., vol. 13, no. 7, pp. 3329-3333, 2013.
- [258] T. Y. Tsang, "Optical third-harmonic generation at interfaces," Phys. Rev. A, vol. 52, no. 5, p. 4116, 1995.
- [259] L. Karvonen, et al., "Investigation of second-and third-harmonic generation in few-layer gallium selenide by multiphoton microscopy," Sci. Rep., vol. 5, no. 1, p. 10334, 2015.
- [260] E. S. Kadantsev and P. Hawrylak, "Electronic structure of a single MoS<sub>2</sub> monolayer," Solid State Commun., vol. 152, no. 10, pp. 909 - 913, 2012.
- [261] F. Zahid, L. Liu, Y. Zhu, J. Wang, and H. Guo, "A generic tight-binding model for monolayer, bilayer and bulk MoS2," AIP Adv., vol. 3, no. 5, 2013. https://doi.org/10.1063/1.4804936.
- [262] A. Kormányos, V. Zólyomi, N. D. Drummond, P. Rakyta, G. Burkard, and V. I. Fal'ko, "Monolayer MoS<sub>2</sub>: trigonal warping, the  $\Gamma$  valley, and spin-orbit coupling effects," *Phys. Rev. B Condens.* Matter Mater. Phys., vol. 88, no. 4, p. 045416, 2013.
- [263] H. Rostami, R. Roldán, E. Cappelluti, R. Asgari, and F. Guinea, "Theory of strain in single-layer transition metal dichalcogenides," Phys. Rev. B, vol. 92, no. 19, p. 195402, 2015.
- [264] H. Rostami, R. Asgari, and F. Guinea, "Edge modes in zigzag and armchair ribbons of monolayer MoS<sub>2</sub>," *J. Phys.: Condens. Matter*, vol. 28, no. 49, p. 495001, 2016.
- [265] H. Rostami, A. G. Moghaddam, and R. Asgari, "Effective lattice Hamiltonian for monolayer MoS<sub>2</sub>: tailoring electronic structure with perpendicular electric and magnetic fields," Phys. Rev. B Condens. Matter Mater. Phys., vol. 88, no. 8, p. 085440, 2013.
- [266] J. Shi, et al., "Giant enhancement and directional second harmonic emission from monolayer WS2 on silicon substrate via Fabry-Pérot micro-cavity," ACS Nano, vol. 16, no. 9, pp. 13933-13941, 2022.
- [267] T. Tong, et al., "Giant second harmonic generation in supertwisted WS<sub>2</sub> spirals grown in step-edge particle-induced

- non-euclidean surfaces," ACS Nano, vol. 18, no. 33, pp. 21939-21947, 2024.
- [268] C. Klingshirn, "The luminescence of ZnO under high one-and two-quantum excitation," Phys. Status Solidi B, vol. 71, no. 2, pp. 547-556, 1975.
- [269] H. Ryu, et al., "Role of the A-site cation in low-temperature optical behaviors of APbBr3 (A = Cs, CH<sub>3</sub>NH<sub>3</sub>)," *J. Am. Chem. Soc.*, vol. 143, no. 5, pp. 2340 - 2347, 2021.
- [270] B. Redding, M. A. Choma, and H. Cao, "Speckle-free laser imaging using random laser illumination," Nat. Photonics, vol. 6, no. 6, pp. 355 - 359, 2012.
- [271] Y. Liu, et al., "Surface-emitting perovskite random lasers for speckle-free imaging," ACS Nano, vol. 13, no. 9, pp. 10653-10661, 2019.
- [272] R. Komissarov, V. Kozlov, D. Filonov, and P. Ginzburg, "Partially coherent radar unties range resolution from bandwidth limitations," Nat. Commun., vol. 10, no. 1, p. 1423, 2019.
- [273] T. H. Nguyen, M. E. Kandel, M. Rubessa, M. B. Wheeler, and G. Popescu, "Gradient light interference microscopy for 3D imaging of unlabeled specimens," Nat. Commun., vol. 8, no. 1, p. 210, 2017.
- [274] I. Khan, M. Leguime, M. Zerrad, and C. Amra, "Detection of ultralow light power back-reflected or back-scattered by optical components using balanced low-coherence interferometry," Phys. Rev. Appl., vol. 16, no. 4, p. 044055, 2021.
- [275] G. Rainò, M. A. Becker, M. I. Bodnarchuk, R. F. Mahrt, M. V. Kovalenko, and T. Stöferle, "Superfluorescence from lead halide perovskite quantum dot superlattices," Nature, vol. 563, no. 7733, pp. 671-675, 2018.
- [276] M. Biliroglu, et al., "Room-temperature superfluorescence in hybrid perovskites and its origins," Nat. Photonics, vol. 16, no. 4, pp. 324-329, 2022.
- [277] K. Huang, K. K. Green, L. Huang, H. Hallen, G. Han, and S. F. Lim, "Room-temperature upconverted superfluorescence," Nat. Photonics, vol. 16, no. 10, pp. 737-742, 2022.
- [278] K. Wu, Y. S. Park, J. Lim, and V. I. Klimov, "Towards zero-threshold optical gain using charged semiconductor quantum dots," Nat. Nanotechnol., vol. 12, no. 12, pp. 1140-1147, 2017.
- [279] D. H. Kim, et al., "High-efficiency electroluminescence and amplified spontaneous emission from a thermally activated delayed fluorescent near-infrared emitter," Nat. Photonics, vol. 12, no. 2, pp. 98-104, 2018.
- [280] H. Sun, et al., "Stimulated emission induced by exciton—exciton scattering in ZnO/ZnMgO multiquantum wells up to room temperature," Appl. Phys. Lett., vol. 77, no. 26, pp. 4250-4252,
- [281] Y. Liang, C. Li, Y. Z. Huang, and Q. Zhang, "Plasmonic nanolasers in on-chip light sources: prospects and challenges," ACS Nano, vol. 14, no. 11, pp. 14375-14390, 2020.
- [282] T. Ahmed, J. Zha, K. K. Lin, H. Kuo, C. Tan, and D. Lien, "Bright and efficient light-emitting devices based on 2D transition metal dichalcogenides," Adv. Mater., vol. 35, no. 31, p. 2208054, 2023.
- [283] Z. Wang, et al., "Two-dimensional light-emitting materials: preparation, properties and applications," Chem. Soc. Rev., vol. 47, no. 16, pp. 6128-6174, 2018.
- [284] Y. Zhu, X. Sun, Y. Tang, L. Fu, and Y. Lu, "Two-dimensional materials for light emitting applications: achievement, challenge and future perspectives," Nano Res., vol. 14, no. 14, pp. 1912-1936, 2021.

- [285] L. Loh, J. Wang, M. Grzeszczyk, M. Koperski, and G. Eda, "Towards quantum light-emitting devices based on van der Waals materials," Nat. Rev. Electr. Eng., pp. 1-15, 2024, https://doi.org/ 10.1038/s44287-024-00108-8.
- [286] F. Withers, et al., "Light-emitting diodes by band-structure engineering in van der Waals heterostructures," Nat. Mater., vol. 14, no. 3, pp. 301-306, 2015.
- [287] B. W. H. Baugher, H. O. H. Churchill, Y. Yang, and P. Jarillo-Herrero, "Optoelectronic devices based on electrically tunable p-n diodes in a monolayer dichalcogenide," Nat. Nanotechnol., vol. 9, no. 4, pp. 262-267, 2014.
- [288] S. Z. Uddin, N. Higashitarumizu, H. Kim, E. Rabani, and A. Javey, "Engineering exciton recombination pathways in bilayer WSe2 for bright luminescence," ACS Nano, vol. 16, no. 1, pp. 1339-1345,
- [289] S. Wang, et al., "Efficient carrier-to-exciton conversion in field emission tunnel diodes based on MIS-type van der Waals heterostack," Nano Lett., vol. 17, no. 8, pp. 5156-5162
- [290] S. Wang, et al., "Light-emitting diodes based on intercalated transition metal dichalcogenides with suppressed efficiency roll-off at high generation rates," Nat. Electron., vol. 8, pp. 56-65, 2024.
- [291] J. Dang, et al., "Electrical switching of spin-polarized light-emitting diodes based on a 2D CrI3/hBN/WSe2 heterostructure," Nat. Commun., vol. 15, no. 1, p. 6799, 2024.
- [292] M. Amani, et al., "Near-unity photoluminescence quantum yield in MoS<sub>2</sub>," *Science*, vol. 350, no. 6264, pp. 1065 – 1068, 2015.
- [293] Y. Lee, et al., "Boosting quantum yields in two-dimensional semiconductors via proximal metal plates," Nat. Commun., vol. 12, no. 1, p. 7095, 2021.
- [294] H. Kim, S. Z. Uddin, N. Higashitarumizu, E. Rabani, and A. Javey, "Inhibited nonradiative decay at all exciton densities in monolayer semiconductors," Science, vol. 373, no. 6553, pp. 448-452, 2021.
- [295] H. Henck, et al., "Light sources with bias tunable spectrum based on van der Waals interface transistors," Nat. Commun., vol. 13, no. 1, p. 3917, 2022.
- [296] I. Kwon, et al., "Multioperation-mode light-emitting field-effect transistors based on van der Waals heterostructure," Adv. Mater., vol. 32, no. 43, p. 2003567, 2020.

- [297] J. C. Shin, et al., "Electrically confined electroluminescence of neutral excitons in WSe2 light-emitting transistors," Adv. Mater., vol. 36, no. 14, p. 2310498, 2024.
- [298] N. Gupta, et al., "Bright mid-wave infrared resonant-cavity light-emitting diodes based on black phosphorus," Nano Lett., vol. 22, no. 3, pp. 1294-1301, 2022.
- [299] J. Gu, B. Chakraborty, M. Khatoniar, and V. M. Menon, "A room-temperature polariton light-emitting diode based on monolayer WS<sub>2</sub>," Nat. Nanotechnol., vol. 14, no. 11, pp. 1024-1028, 2019.
- [300] S. B. Anantharaman, K. Jo, and D. Jariwala, "Exciton photonics: from fundamental science to applications," ACS Nano, vol. 15, no. 8, pp. 12628-12654, 2021.
- [301] J. F. Gonzalez Marin, et al., "Room-temperature electrical control of polarization and emission angle in a cavity-integrated 2D pulsed LED," Nat. Commun., vol. 13, no. 1, p. 4884, 2022.
- [302] M. Turunen, et al., "Quantum photonics with layered 2D materials," Nat. Rev. Phys., vol. 4, no. 4, pp. 219-236,
- [303] C. Palacios-Berraquero and C. Palacios-Berraquero, "Atomically-thin quantum light emitting diodes," in Quantum Confined Excitons in 2-Dimensional Materials, C. Palacios-Berraquero, Ed., Cham, Springer International Publishing, 2018, pp. 71-89.
- [304] S. Schwarz, et al., "Electrically pumped single-defect light emitters in WSe<sub>2</sub>," 2D Mater., vol. 3, no. 2, p. 025038, 2016.
- [305] G. Clark, et al., "Single defect light-emitting diode in a van der Waals heterostructure," Nano Lett., vol. 16, no. 6, pp. 3944-3948, 2016
- [306] J. P. So, et al., "Electrically driven strain-induced deterministic single-photon emitters in a van der Waals heterostructure," Sci. Adv., vol. 7, no. 43, p. eabj3176, 2021.
- [307] B. Schuler, et al., "Electrically driven photon emission from individual atomic defects in monolayer WS2," Sci. Adv., vol. 6, no. 38, p. eabb5988, 2020.
- [308] S. Guo, S. Germanis, T. Taniguchi, K. Watanabe, F. Withers, and I. J. Luxmoore, "Electrically driven site-controlled single photon source," ACS Photonics, vol. 10, no. 8, pp. 2549 – 2555, 2023.
- [309] T. T. H. Do. et al., "Room-temperature strong coupling in a single-photon emitter-metasurface system," Nat. Commun., vol. 15, no. 1, p. 2281, 2024.